Available online at www.sciencedirect.com
ScienceDirect
International Journal of Solids and Structures 44 (2007) 8457–8492
INTERNATIONAL JOURNAL OF SOLIDS AND STRUCTURES
www.elsevier.com/locate/ijsolstr

Numerical analysis for a crack in piezoelectric material under impact

Shuling Hu [a], Shengping Shen [a,*], Toshihisa Nishioka [b]

[a] *MOE Key Laboratory for Strength and Vibration, School of Aerospace, Xi'an Jiaotong University, 28 West Xianning Road, Xi'an, Shaanxi 710049, PR China*

[b] *Simulation Engineering Laboratory, Department of Ocean Mechanical Engineering, Kobe University, 5-1-1 Fukae Minamimachi Higashinada-ku, Kobe 658-0022, Japan*

Received 18 July 2006; received in revised form 16 June 2007
Available online 28 July 2007

Abstract

In this paper, a numerical analysis of impact interfacial fracture for a piezoelectric bimaterial is provided. Starting from the basic equilibrium equation, a dynamic electro-mechanical FEM formulation is briefly presented. Then, the path-independent separated dynamic J integral is extended to piezoelectric bimaterials. Based on the relationship of the path-independent dynamic J integral and the stress and electric displacement intensity factors, the component separation method is used to calculate the stress and electric displacement intensity factors for piezoelectric bimaterials in this finite-element analysis. The response curves of the dynamic J integral, the stress and electric displacement intensity factors are obtained for both homogeneous material (PZT-4 and CdSe) and CdSe/PZT-4 bimaterial. The influences of the piezoelectricity and the electro-mechanical coupling factor on these responses are discussed. The effects of an applied electric field are also discussed.

Keywords: Piezoelectric; Interfacial crack; Dynamic J integral; Finite element analysis

1. Introduction

Piezoelectric materials are of great importance in aerospace, automotive, medical and electronic technologies. Interfacial fracture for piezoelectric materials has received much attention in the last few years (McMeeking, 1999), since interfacial crack is one of the most commonly observed failure modes in piezoelectric laminates, which are used in many modern structures. Various theoretical results have been obtained to understand the interfacial fracture behavior of piezoelectric materials. Most of the analyses are quasi-static (Kuo and Barnett, 1991; Suo et al., 1992; Shen and Kuang, 1998). Applications of piezoelectric materials in the areas of electromechanical devices and electronic packaging illustrate the fact that the transient response of interfa-

* Corresponding author.
E-mail address: sshen@mail.xjtu.edu.cn (S. Shen).

0020-7683/$ - see front matter © 2007 Elsevier Ltd. All rights reserved.
doi:10.1016/j.ijsolstr.2007.06.032

cial crack to impact loading is an important phenomenon and, hence, cannot be neglected (Khutoryansky and Sosa, 1995). Some studies have been carried out for dynamic fracture in homogeneous piezoelectric materials. Shindo and Ozawa (1990) and Parton and Kudriavtsev (1988) analyzed the interaction of piezoelectric harmonic waves with cracks. Dascalu and Maugin (1995) investigated steady-state crack propagation in piezoelectric materials. Li and Mataga (1996a,b) studied the semi-infinite propagating crack in a piezoelectric material with electrode boundary condition and vacuum condition on the crack surface. Shen et al. (1999) analyzed the interfacial crack in piezoelectric bimaterial system under impact loading on the crack surfaces by means of the integral transforms. Nishioka and Shen (2001) obtained the asymptotic transient structure of the near-tip field in a piezoelectric bimaterial containing an interfacial crack under electric/mechanical impact loading, *etc*.

In these researches the dynamic piezoelectric fracture problem is considered in the quasi-electrostatic approximation. That is, the inertial effects are taken into account while keeping the static approximation for the electric fields. This approximation is relevant for the description of the acoustic effects in piezoelectric materials, for which the electromagnetic coupling is not important (Li and Mataga, 1996a). In this paper, we also adopt this assumption.

For dynamic fracture mechanics, Nishioka and Atluri (1983) derived the path-independent dynamic J integral, which has the physical significance of energy release rate. Furthermore, for dynamic interfacial fracture mechanics, Nishioka and Yasin (1999) developed the separated dynamic J integrals, which are equivalent with the separated energy release rates from individual material sides. The separated dynamic J integrals should be very useful to identify the fracture mechanics effects of individual material in an inhomogeneous materials system.

In early works on extracting mixed-mode stress intensity factors for interfacial cracks, Yau and Wang's M integral method (1984) is commonly used. However, it is sometimes difficult to set up the auxiliary solution field that is necessary in this method. The component separation method was extended to static and dynamic interfacial crack problems in both general and piezoelectric materials by Nishioka and his colleagues (Nishioka et al., 2003; Shen and Nishioka, 2003). This method has great advantages over the M integral method, since no auxiliary solution field is needed.

Due to the practical and academic importance of impact interfacial fracture mechanics, this paper deals with loads that are applied suddenly to bimaterials containing interfacial crack. To attempt some progress on this task, a numerical analysis of impact interfacial fracture for a piezoelectric bimaterial is provided. Starting from the basic equilibrium equation, a dynamic electro-mechanical FEM formulation is briefly presented. Then, the path-independent separated dynamic J integral is extended to piezoelectric bimaterials. Based on these asymptotic fields (Nishioka and Shen, 2001) the relationship between the path-independent dynamic J integral and the stress and electric displacement intensity factors are obtained. By appealing to this relationship, the component separation method is used to calculate the stress and electric displacement intensity factors for piezoelectric bimaterials in the finite-element analysis. The response curves of the dynamic J integral and the stress and electric displacement intensity factors are obtained for homogeneous and bimaterial. Two piezoelectric materials, PZT-4 and CdSe are considered in this numerical analysis. These two materials represent two typical piezoelectric materials: PZT-4 for the materials with the stronger electromechanical coupling effect and CdSe those with the lower one, respectively. The electromechanical coupling factor has strong effect on the impact response of piezoelectric materials. The influences of the piezoelectricity and the electromechanical coupling factor on these responses are discussed. The effects of an applied electric field are also discussed.

2. Formulation of electro-mechanical coupled finite element method

Based on the virtual work principle, for the real solution of the electro-mechanical system in the domain V with the boundary ∂V, the following variational equation exists

$$\int_V [(\sigma_{ij,i} + f_j - \rho\ddot{u}_j)\delta u_j + (D_{i,i} - p^e)\delta\phi]\,\mathrm{d}V - \int_{S^\sigma} (\sigma_{ij}n_i - T_j)\delta u_j\,\mathrm{d}s - \int_{S^D} (D_i n_i - p^0)\delta\phi\,\mathrm{d}s = 0 \tag{1}$$

where u_i, ϕ, σ_{ij}, D_i, f_i and p^e are the displacement vector, electric potential, stress tensor, electric displacement vector, body force and body electric charge (i.e. the density of free charge per unite volume), respectively. Throughout, we take $p^e = 0$. Therefore, there are no Coulomb forces acting on free charge within the material. The effect of forces acting on bound charges involved in the polarization process is accounted for in the stored energy of the polarized state (see McMeeking, 1999). Hence, the body force f_i is pure 'material', the contribution from Columbic sources (Maxwell stress) is zero. S^σ denotes the part of the boundary where traction is prescribed, S^D the part of the boundary where charge is prescribed and ρ is the density. T_j is the surface force and p^0 is the surface electric charge, n_i is the normal of the surface. It is also noted that some of these external loads could be due to electrostatic Coulomb forces acting on the free charges at interfaces with electrodes or other surfaces, however, these are small and can be neglected (McMeeking, 1999; Eringen and Maugin, 1990, *etc.*).

Applying the generalized Green–Gauss theorem in conjunction with the constitutive equation (see Appendix A) and the linear geometry Eq. (1) can be written as

$$\delta\left\{\int_V\left[\frac{1}{2}c_{ijkl}\varepsilon_{kl}\varepsilon_{ij} - e_{ijk}E_k\varepsilon_{ij} - \frac{1}{2}\kappa_{ij}E_iE_j\right]\mathrm{d}V\right\} + \int_V \rho\ddot{u}_j\delta u_j\,\mathrm{d}V - \int_V f_j\delta u_j\,\mathrm{d}V - \int_{S^\sigma} T_j\delta u_j\,\mathrm{d}s - \int_{S^D} p^0\delta\phi\,\mathrm{d}s = 0 \tag{2}$$

where ε_{ij} is the strain tensor and E_i is the electric field vector, c_{ijkl} is elastic constants, κ_{ij} is the dielectric permittivities and e_{ijk} is the piezoelectric constants.

The continuous displacement and potential are interpolated in terms of j nodal values as

$$u_i = \sum_{j=1}^{n} N_j u_i^{(j)},\ \phi = \sum_{j=1}^{n} N_j\phi^{(j)} \tag{3}$$

where N_j are interpolation functions. Differentiating Eq. (3) yields expressions for the strains and electric field (negative potential gradient)

$$\varepsilon = \mathbf{B}_u\mathbf{u},\quad \mathbf{E} = -\mathbf{B}_\phi\phi \tag{4}$$

If we let N be the total element number of the system, then, the final equation can be obtained as

$$\sum_{e=1}^{N}\left\{\mathbf{M}_e\ddot{\mathbf{Q}}_e + \mathbf{K}_e\mathbf{Q}_e\right\} = \sum_{e=1}^{N}\mathbf{F}_e \quad \text{i.e. } \mathbf{M}\ddot{\mathbf{Q}} + \mathbf{K}\mathbf{Q} = \mathbf{F} \tag{5}$$

where $\mathbf{Q}_e$ contains the displacement as well as the electric potential degrees of freedom of a finite element, $\mathbf{K}_e$ is the element stiffness matrix, $\mathbf{M}_e$ is kinematically consistent mass matrix, and $\mathbf{F}_e$ is the load vector,

$$\mathbf{M}_e = \begin{bmatrix}\int_{V_e}\rho\mathbf{N}^{\mathrm{T}}\mathbf{N}\,\mathrm{d}V & 0\\ 0 & 0\end{bmatrix},\quad \mathbf{K}_e = \begin{bmatrix}\mathbf{K}_e^{(u)} & \mathbf{K}_e^{(u\phi)}\\ \mathbf{K}_e^{(\phi u)} & \mathbf{K}_e^{(\phi)}\end{bmatrix}\quad \mathbf{F}_e = \begin{bmatrix}\int_{V_e}\mathbf{N}^{\mathrm{T}}\mathbf{f}\,\mathrm{d}V & 0\\ 0 & 0\end{bmatrix} + \begin{bmatrix}\int_{S_e^\sigma}\mathbf{N}^{\mathrm{T}}\mathbf{T}\,\mathrm{d}s\\ \int_{S_e^D}\mathbf{N}^{\mathrm{T}}p^0\,\mathrm{d}s\end{bmatrix} \tag{6}$$

in which $\mathbf{N}$ is the matrix containing the shape functions of displacements (3), and

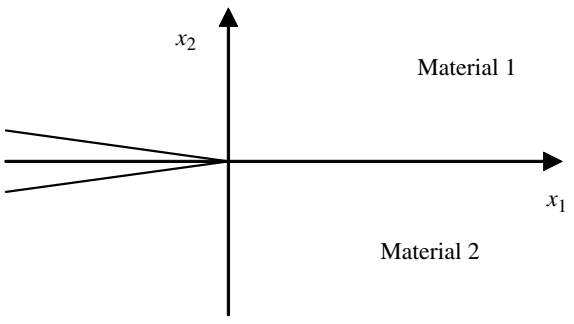

Fig. 1. An interface crack.

$$\mathbf{K}_e^{(\phi)} = \int_{V^e} \mathbf{B}_u^{\mathrm{T}} \mathbf{c} \mathbf{B}_u \, \mathrm{d}V, \quad \mathbf{K}_e^{(u\phi)} = \int_{V^e} \mathbf{B}_u^{\mathrm{T}} \mathbf{e}^{\mathrm{T}} \mathbf{B}_\phi \, \mathrm{d}V$$
$$\mathbf{K}_e^{(\phi u)} = \int_{V^e} \mathbf{B}_\phi^{\mathrm{T}} \mathbf{e} \mathbf{B}_u \, \mathrm{d}V, \quad \mathbf{K}_e^{(\phi)} = -\int_{V^e} \mathbf{B}_\phi^{\mathrm{T}} \kappa \mathbf{B}_\phi \, \mathrm{d}V \tag{7}$$

Eight-node isoparametric elements are used in the analysis. The Newmark method is used for the time integration of Eq. (5). The final form to be solved for FEM can be expressed by

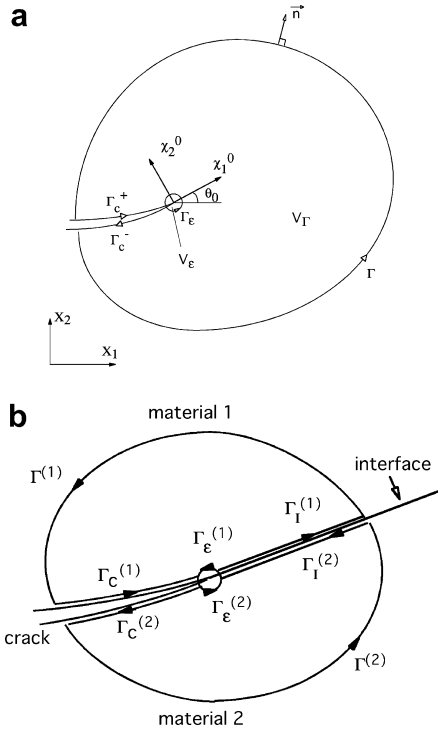

Fig. 2. Definition of integral paths: (a) crack in homogeneous material; (b) interfacial crack in inhomogeneous material.

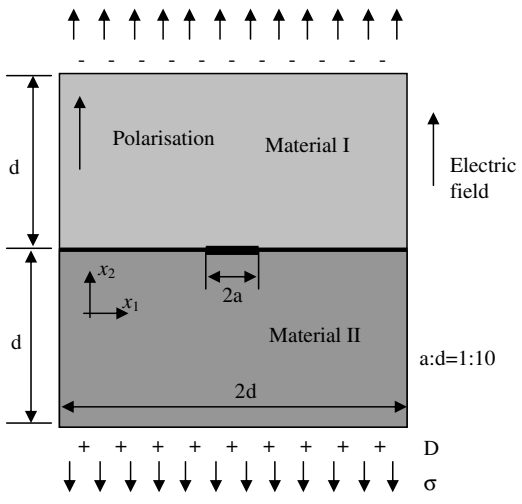

Fig. 3. Piezoelectric interfacial crack.

$$a_0(\mathbf{M}+\mathbf{K})\mathbf{Q}_n = \mathbf{F}_n + \mathbf{M}(a_0\mathbf{Q}_{n-1} + a_2\dot{\mathbf{Q}}_{n-1} + a_3\ddot{\mathbf{Q}}_{n-1}) \tag{8}$$

The subscripts n and $n-1$ denote the nodal quantities at the current step n and at the previous step $n-1$, respectively. After determining the nodal displacement vector at the current time step, the nodal velocities and accelerations can be determined by

$$\begin{aligned}\ddot{\mathbf{Q}}_n &= a_0(\mathbf{Q}_n - \mathbf{Q}_{n-1}) - a_2\dot{\mathbf{Q}}_{n-1} - a_3\ddot{\mathbf{Q}}_{n-1}\\ \dot{\mathbf{Q}}_n &= \dot{\mathbf{Q}}_{n-1} + a_6\ddot{\mathbf{Q}}_{n-1} + a_7\ddot{\mathbf{Q}}_n\end{aligned} \tag{9}$$

The coefficients a_0–a_7 are given by

$$\begin{aligned}&a_0 = 1/\{\beta(\Delta t_n)^2\}, \quad a_1 = \delta/(\beta\Delta t_n), \quad a_2 = 1/(\beta\Delta t_n), \quad a_3 = 1/(2\beta) - 1, \quad a_4 = \delta/\beta - 1,\\ &a_5 = (\Delta t_n/2)\{\delta/\beta - 2\}, \quad a_6 = \Delta t_n(1-\delta), \quad a_7 = \delta\Delta t_n\end{aligned} \tag{10}$$

where Δt_n is the time increment, and β and δ are the Newmark's parameters, and $\beta = 1/4$ and $\delta = 1/2$ are chosen to assure the unconditionally stable time integration scheme.

3. Near-tip field, path-independence integral and energy release rate

Fig. 1 shows a planar interfacial crack. Materials 1 and 2 occupy the two half-spaces. The generalized two-dimensional deformation is considered in which the three components of displacement and the electric potential depend only on in-plane coordinates.

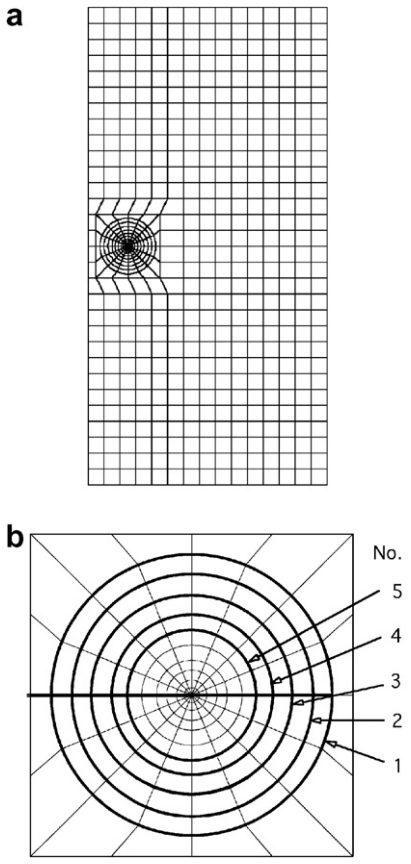

Fig. 4. Mesh pattern and integral paths: (a) mesh pattern (1/2 of the structure, 1410 elements, 4389 nodes); (b) crack tip elements and the integral paths.

For the static crack subjected to impact loading, the stress and electric displacement intensity factors can be expressed in the form as that for static case by Shen and Kuang (1998) as

$$\mathbf{K} \equiv [K_1 \quad K_2 \quad K_3 \quad K_4]^{\mathrm{T}} = \lim_{r\to 0} \sqrt{2\pi r}\, \Lambda\, \mathrm{diag}\left[r^{-\mathrm{i}\varepsilon} \quad r^{\mathrm{i}\varepsilon} \quad r^{-\kappa} \quad r^{\kappa} \right] \cdot \Lambda^{-1} [\sigma_{12} \quad \sigma_{22} \quad \sigma_{23} \quad D_2]^{\mathrm{T}} \tag{11}$$

where r stands for the distance from the crack tip, ε and κ involve the bimaterial constant and crack velocity, $\mathbf{\Lambda}$ is the eigenvector matrix associated with the eigenvalue problem in the Stroh formalism (see Appendix A). The above definition provides a unique characterization of the crack tip (Hwu, 1993; Beom and Atluri, 1996). Due to the oscillatory singularity in the near-tip field, the individual stress and electric displacement intensity factors K_1, K_2, K_3 and K_4 for interfacial crack can not be uniquely associated with mode I, mode II, mode III and mode IV fracture as defined in homogeneous piezoelectric materials. However, K_1, K_2, K_3 and K_4 still represent four different modes of fracture action.

Table 1
Comparison of FEM-results with exact solution for the electromechanical interfacial crack subjected to combined loading

Element No.	r/a	K_1 (MPa m$^{-1/2}$)		K_2 (MPa m$^{-1/2}$)		K_4 (10^{-3} C m$^{-3/2}$)	
		FEM present	Error (%)	FEM present	Error (%)	FEM present	Error (%)
First	0.0375	5.5802×10^{-2}	−2.935	7.9874×10^{-2}	2.134	7.9530×10^{-2}	0.189
Second	0.075	5.7545×10^{-2}	0.096	7.8377×10^{-2}	0.220	7.9523×10^{-2}	0.180
Third	0.125	5.7739×10^{-2}	0.434	7.7993×10^{-2}	−0.271	7.9520×10^{-2}	0.176
Fourth	0.175	5.8084×10^{-2}	1.034	7.7930×10^{-2}	−0.352	7.9521×10^{-2}	0.178
Fifth	0.25	5.8481×10^{-2}	1.724	7.7846×10^{-2}	−0.459	7.9522×10^{-2}	0.179
Exact solution		5.74896×10^{-2}		7.82051×10^{-2}		7.9380×10^{-2}	

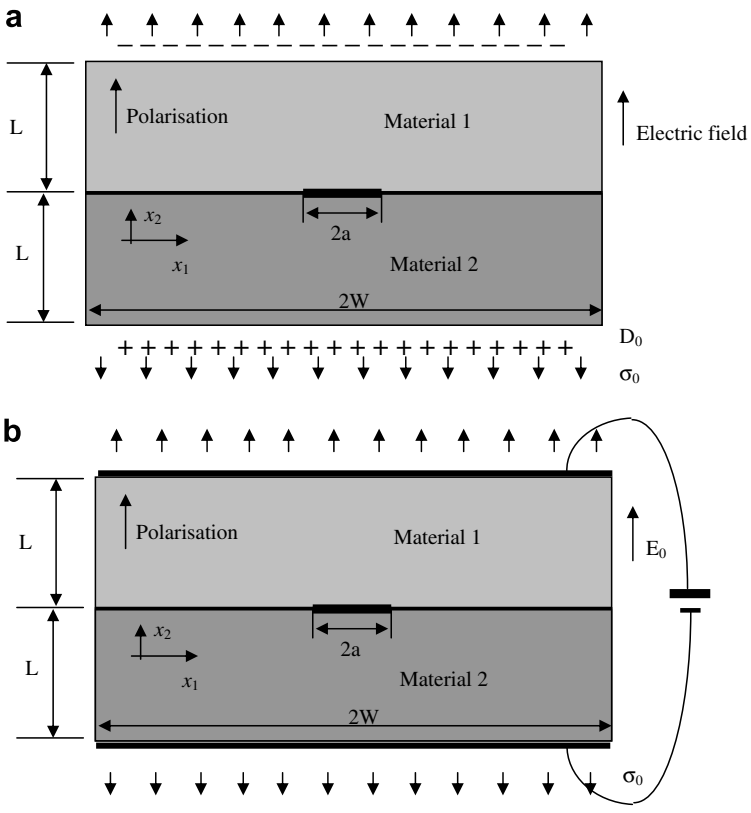

Fig. 5. (a) Case 1; (b) Case 2.

The crack opening displacement and electric potential jump at distance r behind the crack tip can be expressed as

$$[\delta_1 \quad \delta_2 \quad \delta_3 \quad \delta_4]^{\mathrm{T}} = \frac{4\sqrt{r}}{\sqrt{2\pi}}\mathbf{H}\Lambda \cdot \mathrm{diag}\left[r^{\mathrm{i}\varepsilon}\frac{\cosh\pi\varepsilon}{1+2\mathrm{i}\varepsilon} \quad r^{-\mathrm{i}\varepsilon}\frac{\cosh\pi\varepsilon}{1-2\mathrm{i}\varepsilon} \quad r^{\kappa}\frac{\cos\pi\kappa}{1+2\kappa} \quad r^{-\kappa}\frac{\cos\pi\kappa}{1-2\kappa}\right] \cdot \Lambda^{-1}(\mathbf{I}+\bar{\mathbf{H}}^{-1}\mathbf{H})^{-1}[K_1 \quad K_2 \quad K_3 \quad K_4]^{\mathrm{T}} \tag{12}$$

where $\mathbf{H}$ is a Hermitian matrix. The influence of material properties and crack velocity on near-tip fields for interfacial crack depends on the oscillation index ε and κ, and the Hermitian matrix $\mathbf{H}$, to which the eigenvector matrix $\mathbf{\Lambda}$ are related (see Appendix A).

The generalized dynamic J' integral for a linear piezoelectric material can be written as

$$\begin{aligned} J'_k &= \lim_{\Gamma_\varepsilon \to 0} \int_{\Gamma_\varepsilon} [(W+T)n_k - n_i\sigma_{ij}u_{j,k} - n_iD_i\phi_{,k}]\,\mathrm{d}s \\ &= \lim_{\Gamma_\varepsilon \to 0} \left\{ \int_{\Gamma+\Gamma_\mathrm{c}} [(W+T)n_k - n_i\sigma_{ij}u_{j,k} - n_iD_i\phi_{,k}]\,\mathrm{d}s + \int_{V-V_\varepsilon} [\rho\ddot{u}_iu_{i,k} - \rho\dot{u}_i\dot{u}_{i,k}]\,\mathrm{d}V \right\} \end{aligned} \tag{13}$$

where the electric enthalpy density $W = \frac{1}{2}\sigma_{ij}u_{i,j} + \frac{1}{2}D_i\phi_{,i}$ and the kinetic energy density $T = \frac{1}{2}\rho\dot{u}_i\dot{u}_i = \frac{1}{2}\rho c^2u_{i,1}u_{i,1}$. n_i is the unit outward normal vector. Γ_ε is denotes the near field integral path, while Γ and Γ_c are the far field path and the crack face integral path, respectively. Γ connects any two points on opposite sides of the crack surface and enclosing the crack tip and ds is an element of arc length along Γ. The integral paths are defined in Fig. 2(a). Physically, the near-tip region V_ε can be considered as the process zone in which micro-process associated with fracture occur. Eq. (13) is extension of the dynamic elastic version due to Nishioka and Atluri

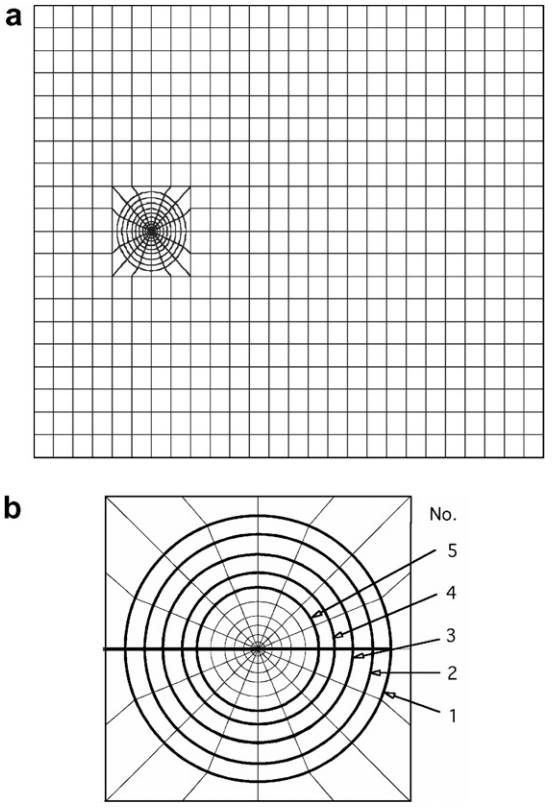

Fig. 6. Mesh pattern and integral paths: (a) mesh pattern (1/2 of the structure, 680 elements, 2899 nodes); (b) crack tip elements and the integral paths.

(1983), it is well known that the generalized dynamic J'_k integrals are independent of any path Γ. The crack-axis components of the dynamic J integral $J_k^{\prime 0}$ can be evaluated by the coordinate transformation:

$$J_k^{\prime 0} = \alpha_{kl} J'_l \tag{14}$$

where α_{kl} is the coordinate transformation tensor. For a two-dimensional case as shown in Fig. 2(a), the tangential component of dynamic J integrals can be expressed by

$$J_1^{\prime 0} = J'_1 \cos\theta_0 + J'_2 \sin\theta_0 \tag{15}$$

The tangential component of the dynamic J integral $J_1^{\prime 0}$ has the physical meaning of energy release rate due to crack extension, i.e., $J_1^{\prime 0} = G$, where G is the energy release rate.

Considering an inhomogeneous piezoelectric system with a dynamically propagating interfacial crack as shown in Fig. 2(b), we extended the separated dynamic J integrals for dynamic elastic to piezoelectric material in Nishioka et al. (2003) as

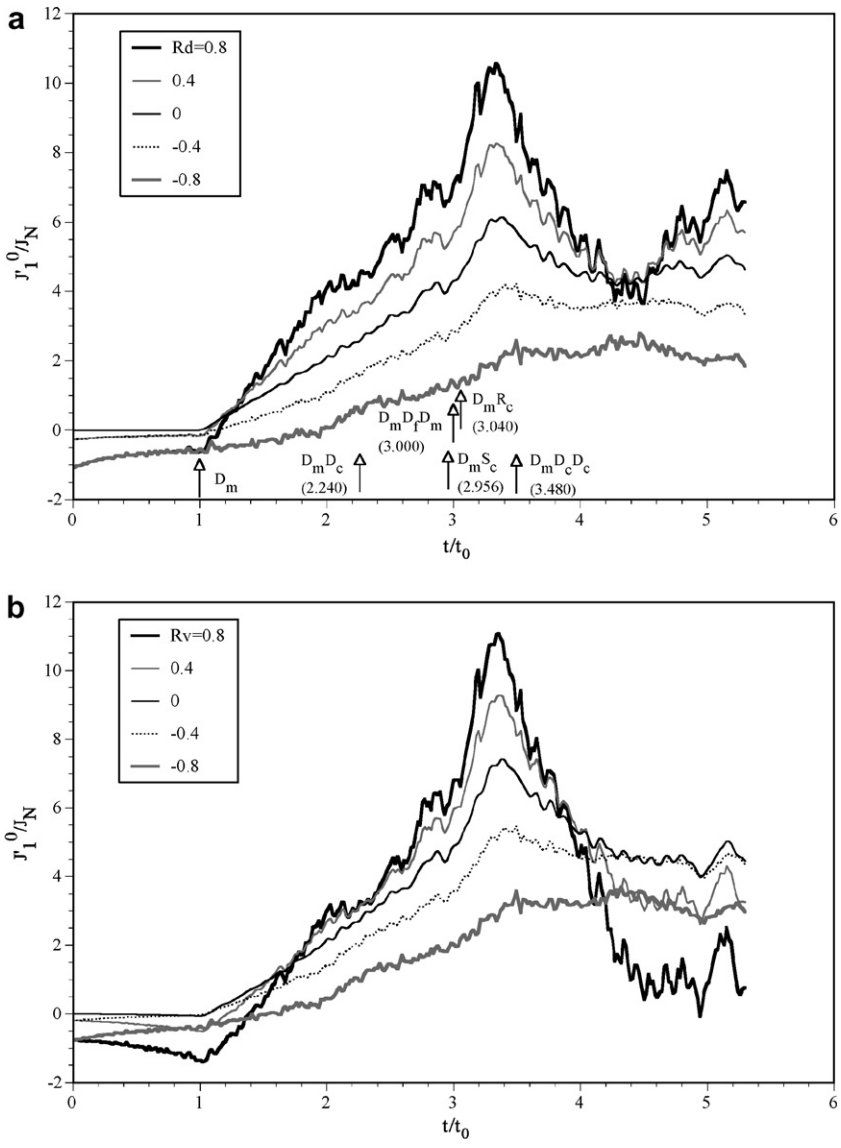

Fig. 7. Dynamic J integral response in PZT-4 plate: (a) for Case 1; (b) for Case 2.

$$
\begin{aligned}
J_k'^{(m)} &= \lim_{\Gamma_\varepsilon^{(m)}\to 0}\int_{\Gamma_\varepsilon^{(m)}}[(W+T)n_k - n_i\sigma_{ij}u_{j,k} - n_iD_i\phi_{,k}]\,\mathrm{d}s \\
&= \lim_{\Gamma_\varepsilon^{(m)}\to 0}\left\{\int_{\Gamma^{(m)}+\Gamma_c^{(m)}+\Gamma_I^{(m)}}[(W+T)n_k - n_i\sigma_{ij}u_{j,k} - n_iD_i\phi_{,k}]\,\mathrm{d}s + \int_{V^{(m)}-V_\varepsilon^{(m)}}[\rho\ddot{u}_iu_{i,k} - \rho\dot{u}_i\dot{u}_{i,k}]\,\mathrm{d}V\right\}
\end{aligned}
\tag{16}
$$

where $m = 1, 2$, $\Gamma_I^{(m)}$ are the integral paths along the interface in sides of the material 1 and 2, respectively. The integral paths are defined in Fig. 2(b). The path independence of the separated dynamic J integrals can be verified in a similar manner in Nishioka and Atluri (1983). The crack-axis components of the separated dynamic J integral can also be evaluated by the coordinate transformation:

$$
J_k'^{0(m)} = \alpha_{kl}J_l'^{(m)} \tag{17}
$$

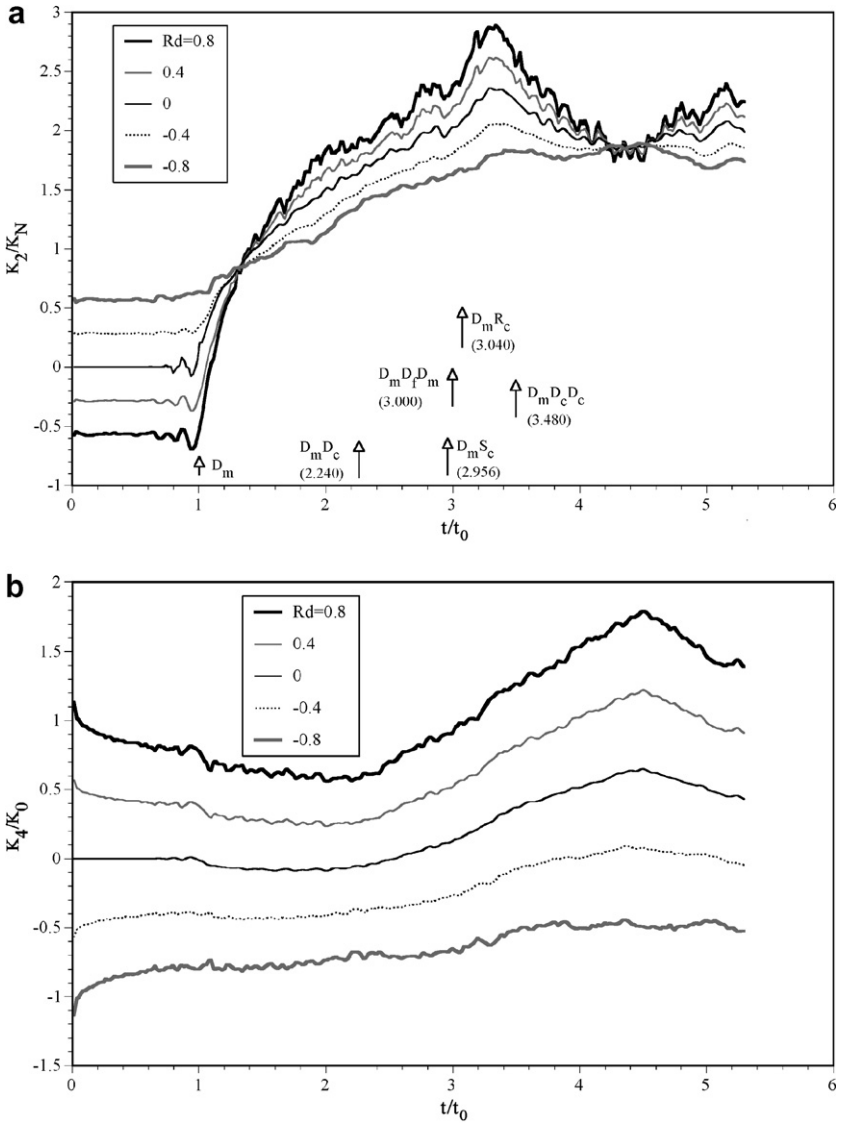

Fig. 8. Responses of the general dynamic SIFs in PZT-4 for Case 1: (a) the stress intensity factor K_2; (b) the electric displacement intensity factor K_4.

The separated dynamic J integrals also have the physical significance of the separated energy release rates $G^{(m)}$ which are the energy flow rates from material m into the propagating interfacial crack tip per unit crack extension. Thus, we have the following relations

$$J_1'^{0(m)} = G^{(m)} = J_1'^{(m)} \cos\theta_0 + J_2'^{(m)} \sin\theta_0 \tag{18}$$

Furthermore, the dynamic J integral and the energy release rate can be obtained by the sum of the separated dynamic J integrals and the separated energy release rate, respectively, as

$$J_1' = J_1'^{0(1)} + J_1'^{0(2)} = G = G^{(1)} + G^{(2)} \tag{19}$$

For a straight crack as shown in Fig. 1, $J_k'^0 = J_k'$ and $J_k'^{0(m)} = J_k'^{(m)}$. Similar to Yeh et al. (1993), the generalized dynamic J' integrals can be written in the complex form for a piezoelectric solid as

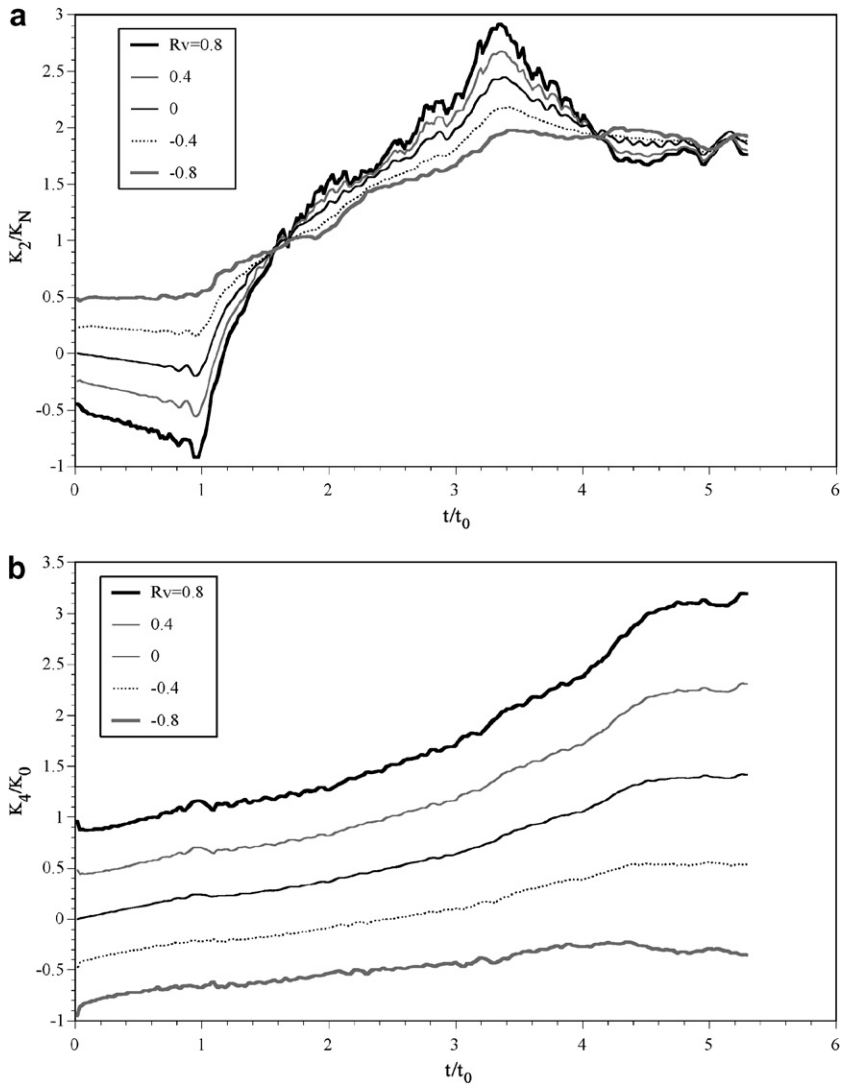

Fig. 9. Responses of the general dynamic SIFs in PZT-4 for Case 2: (a) the stress intensity factor K_2; (b) the electric displacement intensity factor K_4.

$$J_1' = \lim_{\varepsilon\to 0} \mathrm{Re}\left\{\sum_{k=1}^{4}\int_{\Gamma_\varepsilon}[f_k'(z_k)]^2\,\mathrm{d}z_k\right\} = \frac{1}{2}\lim_{\varepsilon\to 0}\int_{\Gamma_\varepsilon}\left\{\mathbf{f}'^{\mathrm{T}}(z)\mathbf{f}'(z) - \bar{\mathbf{f}}'^{\mathrm{T}}(z)\bar{\mathbf{f}}'(z)\right\}\mathrm{d}z \tag{20}$$

where $f_k(z_k)$ are the analytic functions generating the singular part of the interfacial stress and electric displacement (see Appendix A). Thus, the generalized dynamic J_1' integral can be related to the dynamic stress and electric displacement intensity factors as

$$J_1' = G = \frac{1}{4}\mathbf{K}^{\mathrm{T}}\mathbf{U}\mathbf{K} \tag{21}$$

where

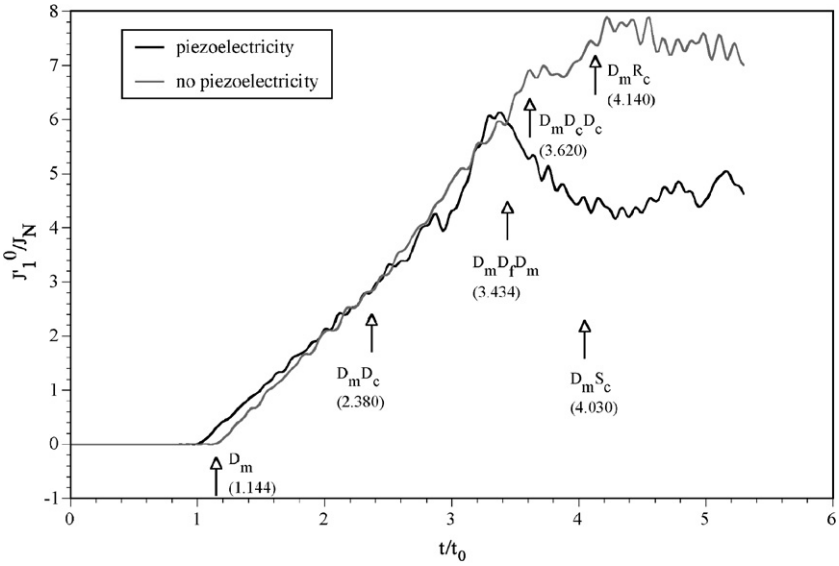

Fig. 10. The influence of piezoelectricity on the response of dynamic J integral in PZT-4 plate.

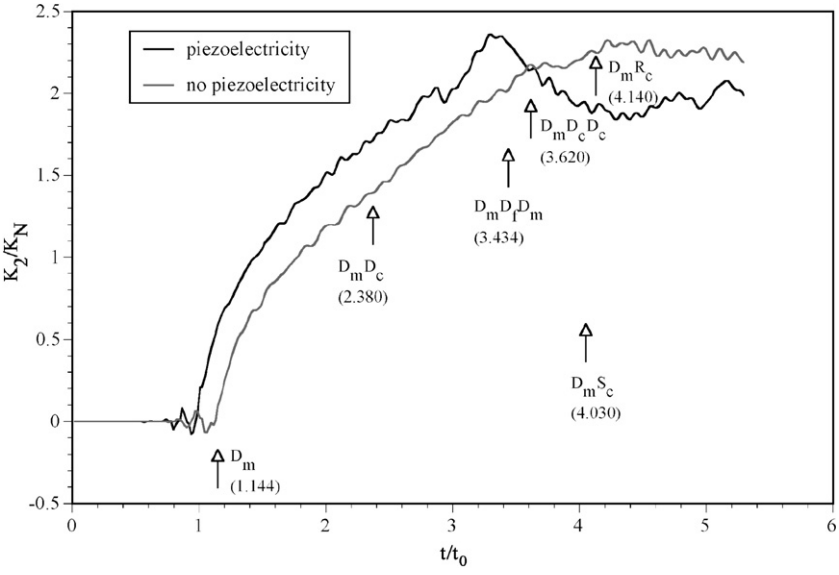

Fig. 11. The influence of piezoelectricity on the response of K_2 in PZT-4 plate.

$$\mathbf{U} = 2(\mathbf{H}^{-1} + \bar{\mathbf{H}}^{-1})^{-1} \tag{22}$$

In many numerical analyses, the far-field integrals are usually used to evaluate the values of the dynamic J integral. In this case it is convenient to consider the following expression of the following expression of the dynamic J integral:

$$J'_k = \int_{\Gamma+\Gamma_c} [(W+T)n_k - n_i\sigma_{ij}u_{j,k} - n_iD_i\phi_{,k}]\,\mathrm{d}s + \int_{V_\Gamma} [\rho\ddot{u}_iu_{i,k} - T_{,k}]\,\mathrm{d}V \tag{23}$$

It is noted that a negative energy release rate can be induced with a large electric field applied in conjunction with a moderate mechanical load. Many fracture criteria have been proposed for piezoelectric materials (Park and Sun, 1995; Gao et al., 1997; McMeeking, 1999; Shen and Nishioka, 2000). However, a conventional

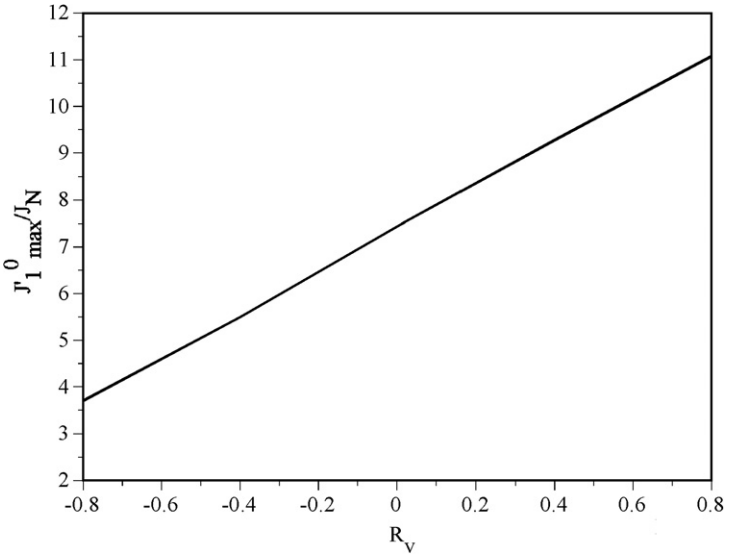

Fig. 12. Variation of the maximum values of dynamic J integral against R_v for PZT-4 plate.

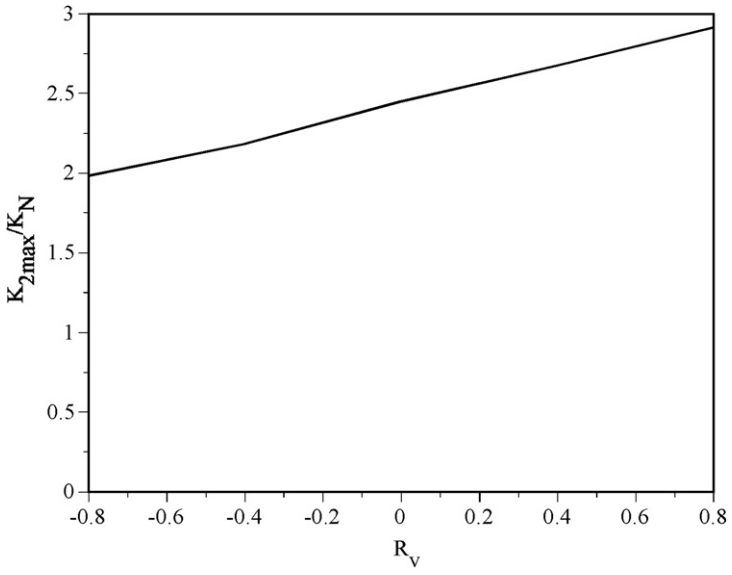

Fig. 13. Variation of the maximum values of K_2 against R_v for PZT-4 plate.

fracture criterion characterized by the total energy release rate in conjunction with the mode mixity can still work, where the mode mixity is defined to be the ratios K_1/K_2, K_3/K_2 and K_4/K_2 at the crack tip. Hence, the fracture condition can be assumed as

$$J_1\left(\frac{K_1}{K_2},\frac{K_3}{K_2},\frac{K_4}{K_2}\right) = G\left(\frac{K_1}{K_2},\frac{K_3}{K_2},\frac{K_4}{K_2}\right) = G_c\left(\frac{K_1}{K_2},\frac{K_3}{K_2},\frac{K_4}{K_2}\right) \tag{24}$$

4. Component separation method

In FEA, although the intensity factors can be obtained directly from the near-tip displacements by means of Eq. (12), the results are not very accurate in many cases. However, the ratios K_1/K_2, K_3/K_2 and K_4/K_2 can be calculated accurately in terms of the ratios of crack surface displacement and electric potential, δ_1/δ_2, δ_3/δ_2 and δ_4/δ_2, by using Eq. (12). Thus, the individual intensity factors K_1, K_2, K_3 and K_4 can be obtained from these ratios K_1/K_2, K_3/K_2 and K_4/K_2 in conjugation with Eq. (21), where the dynamic J integral can be calculated accurately from Eq. (23). This method is called the component separation method of dynamic J integral, which is very convenient in FEM. The details of this method can be found in Nishioka et al. (2003).

5. Verification examples

In order to test the accuracy of the suggested finite element techniques, the methods are applied to a static interfacial crack, because an analytical solution can be employed to evaluate the simulated results. We consider a class of piezoelectric materials of practical significance with the transverse symmetry around the poling-axis x_2. The crack plane perpendicular to the poling-axis, and the anti-plane u_3 decouples from u_1, u_2 and ϕ. We only consider the in-plane deformation and ignored u_3.

A bimaterial system composed of CdSe and PZT-4 with a center crack of length $2a$ subjected to uniform remote tensile $\sigma_{22}^{\infty} = 1$ MPa and electric displacement $D_2^{\infty} = 0.001\ \mathrm{C/m^2}$ is considered. The specimen dimensions, 40×40 mm with a $2a = 4$ mm center crack, and the loading conditions are shown in Fig. 3. The lateral dimensions of the system are much larger than the crack length. The exact analytical solution of stress and

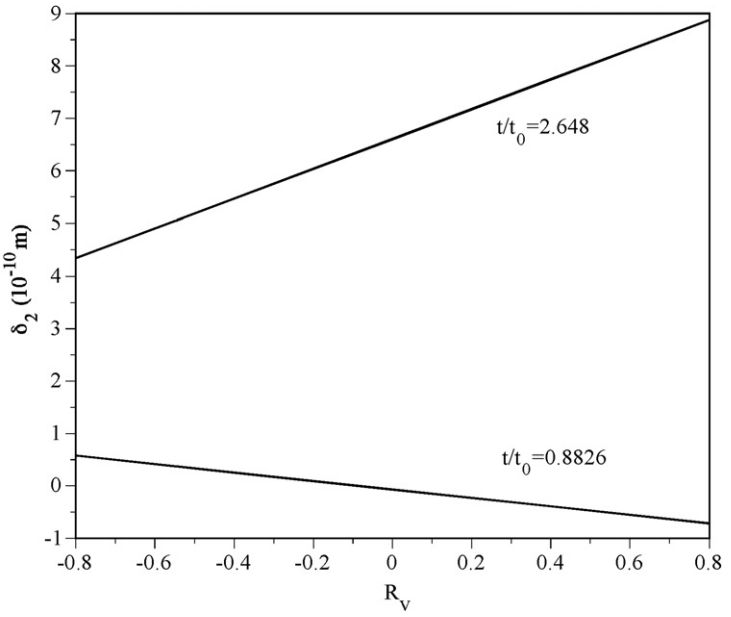

Fig. 14. Variation of the crack opening displacement δ_2 at distance $r = a/3$ behind the crack tip, against R_v for $t/t_0 = 0.8826$ and 2.648 in PZT-4 plate.

electric displacement intensity factors for the infinite plane ($a/d \ll 1$) was given in Shen and Kuang (1998) and Nishioka and Shen (2001).

The finite element mesh, representing the right half of the structure, is shown in Fig. 4 enclosing the crack tip details and the paths to be used for calculating the J integrals. Eight-node isoparametric elements were used in the analysis. For crack tip elements, as in conventional FEM for crack problem, 3 nodes in every crack-tip eight-node isoparametric element are overlapped on the crack tip.

The material parameters for PZT-4 are given below (Shen and Kuang, 1998):

Elastic constants (GPa):
$c_{11} = 139.0$, $c_{12} = 74.3$, $c_{22} = 113.0$, $c_{33} = 25.6$;
Piezoelectric constants (C/m^2):
$e_{21} = -6.98$, $e_{22} = 13.84$, $e_{15} = 13.44$;
Dielectric constants (10^{-9} F/m):
$\kappa_{11} = 6.00$, $\kappa_{22} = 5.47$;
Mass density (kg/m^3):
$\rho = 7600$;

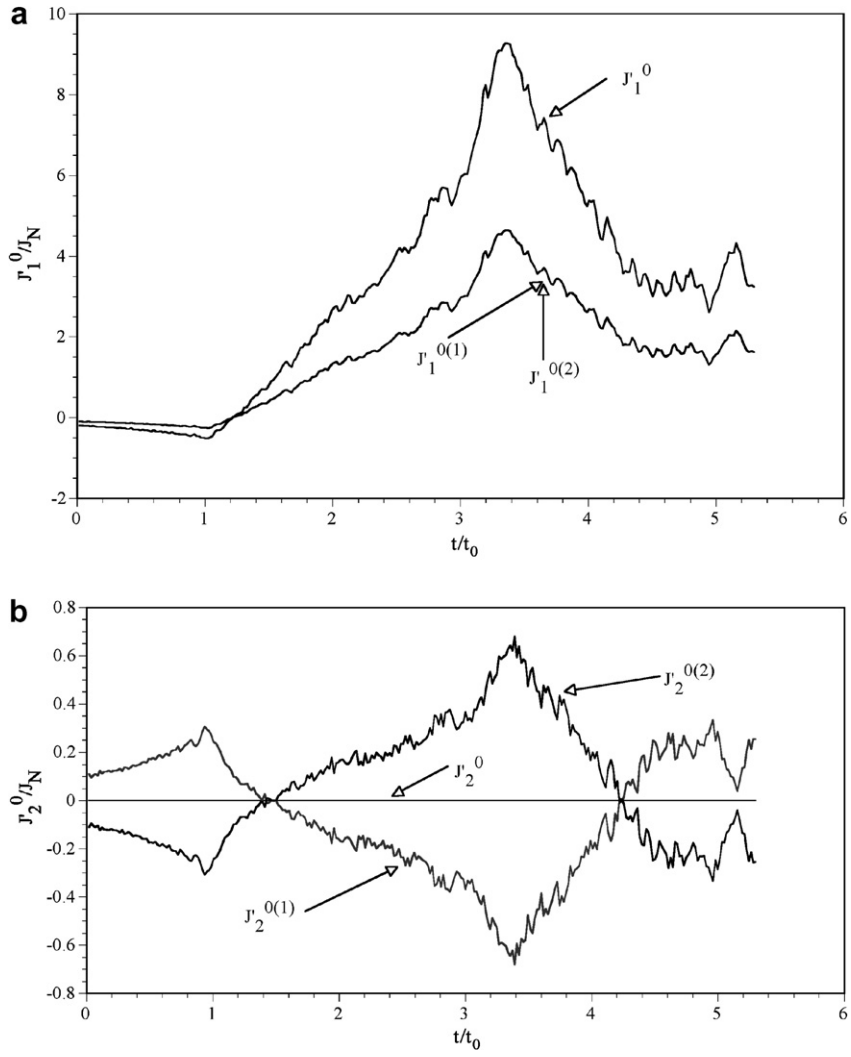

Fig. 15. Responses of separated dynamic J integrals at $R_v = 0.4$ in PZT-4 plate: (a) $J_1^{\prime 0}$; (b) $J_2^{\prime 0}$.

and those for CdSe are (Eringen and Maugin, 1990):

Elastic constants (GPa):
$c_{11} = 73.80$, $c_{12} = 39.86$, $c_{22} = 82.33$, $c_{33} = 12.95$;
Piezoelectric constants (C/m^2):
$e_{21} = 0.162$, $e_{22} = 0.353$, $e_{15} = -0.158$;
Dielectric constants (10^{-9} F/m):
$\kappa_{11} = 0.1145$, $\kappa_{22} = 0.1018$;
Mass density (kg/m^3):
$\rho = 5684$;

where N and C denote, respectively Newton's and Coulombs. Stronger piezoelectric coupling effect can be expected as $|e_{22}/(\kappa_{22}c_{22})^{0.5}| = 0.5567$ for PZT-4, while lower piezoelectric coupling effect can be expected as $|e_{22}/(\kappa_{22}c_{22})^{0.5}| = 0.1221$ for CdSe (lower piezoelectric coupling is present for $|e_{22}/(\kappa_{22}c_{22})^{0.5}| \ll 1$).

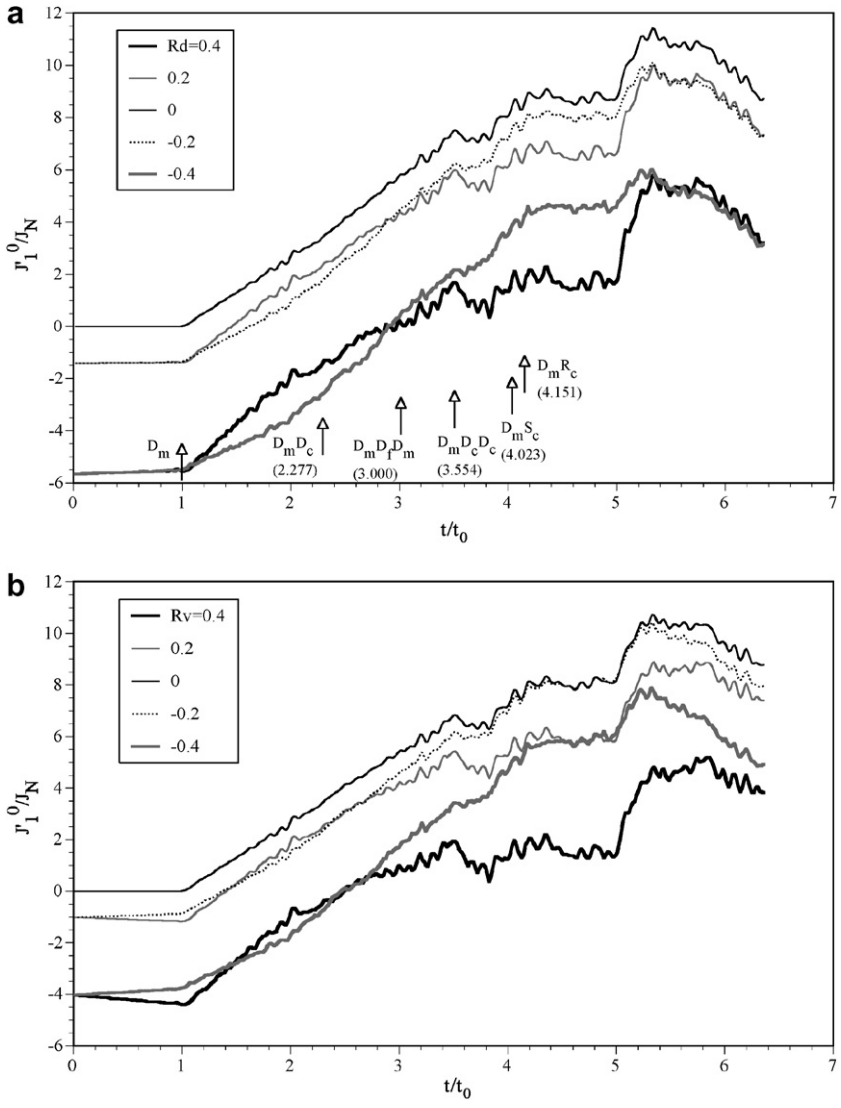

Fig. 16. Dynamic J integral response in CdSe plate: (a) for Case 1; (b) for Case 2.

In this analysis, first, the generalized J integrals are evaluated by Eq. (13) for five circular integral paths (see Fig. 4). Then, these values are converted to the stress and electric displacement intensity factors using the component separation method. Comparisons of the simulated stress and electric displacement intensity factors with analytical result (Shen and Kuang, 1998) are presented in Table 1. Crack opening displacements and electric potential jump are taken from the first five elements behind the crack tip. It is noted that the errors for K_1, K_2 and K_4 are very small if the crack opening displacements and electric potential jump are not taken from the first element. It is shown that relative errors for K_2 and K_4 are below 0.5%, while relative errors for K_1 are less than 2%. It is reasonable to state that the accuracy of the dominant K_i is extremely good. The comparisons shown in Table 1 indicate that the finite element solution is quite accurate. Other examples can also be found in Nishioka and Shen (2001).

6. Impact response of a crack in homogeneous material

In this section, two homogeneous plates, PZT-4 and CdSe plates, with a central crack are considered (see Fig. 5), respectively. These two materials represent two typical piezoelectric materials: PZT-4 for the stronger

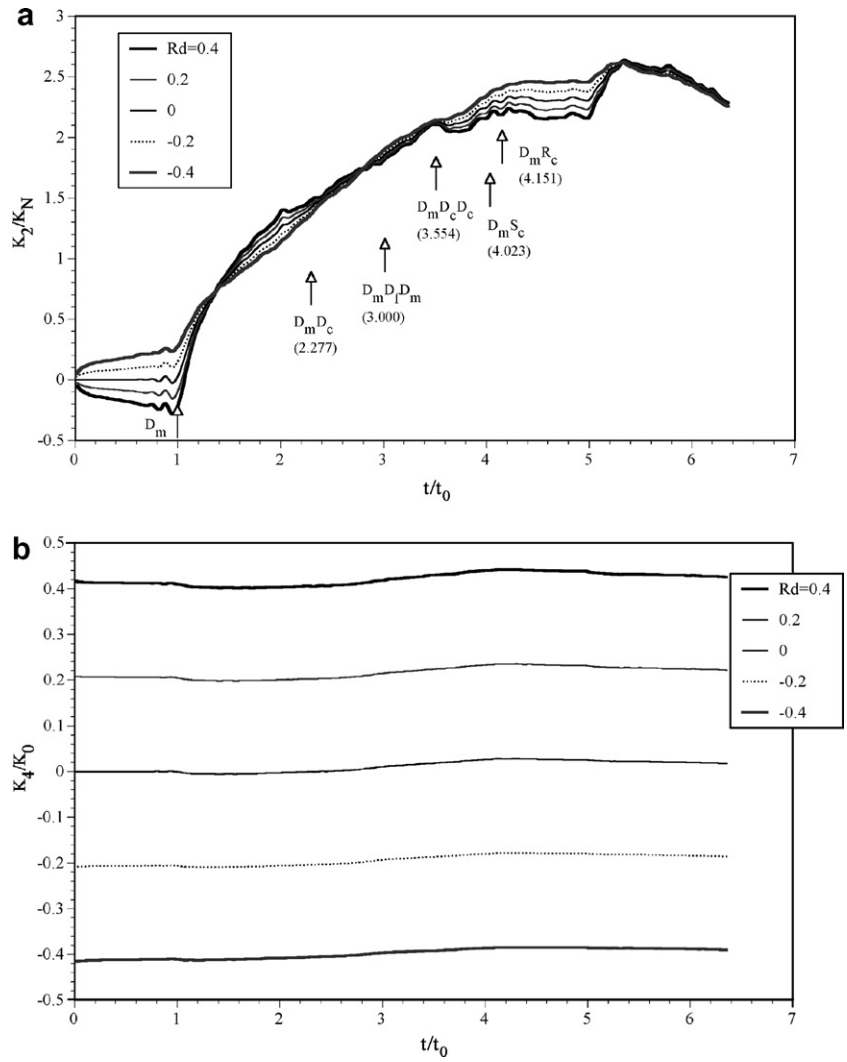

Fig. 17. Responses of the general dynamic SIFs in CdSe for Case 1: (a) the stress intensity factor K_2; (b) the electric displacement intensity factor K_4.

electromechanical coupling effect and CdSe the lower, respectively. We will find that the electromechanical coupling factor affects the impact response of piezoelectric materials strongly.

The plates are subjected to impact mechanical and electric loading of step function type at time $t = 0$. The electric loading can be electric displacement (Case 1) or electric potential (Case 2), as shown in Fig. 5. For Case 2, the electric field is applied by controlling the potential on thin electrodes bonded to the upper $(-V)$ and lower $(+V)$ surfaces of the specimen where V is the magnitude of the applied potential. The dimensions of the plates are $2W = 104$ mm, $2L = 40$ mm and the crack length $2a = 24$ mm. The finite element mesh is shown in Fig. 6 enclosing the crack tip details and the paths to be used for calculating the J integral. In fact, it is enough to analyze a quarter of the model due to the symmetry in both horizontal and vertical direction. However, to make a comparison with the bimaterial model, the right half part of the plate is analyzed only using its vertical symmetry. Eight-node isoparameter elements are used. In this section, the time step is taken to be 0.08×10^{-6} s.

The elastic stress wave velocities of this class of piezoelectric materials, which has transverse symmetry around the poling-axis x_2 can be calculated as(Sun and Zhang, 1984)

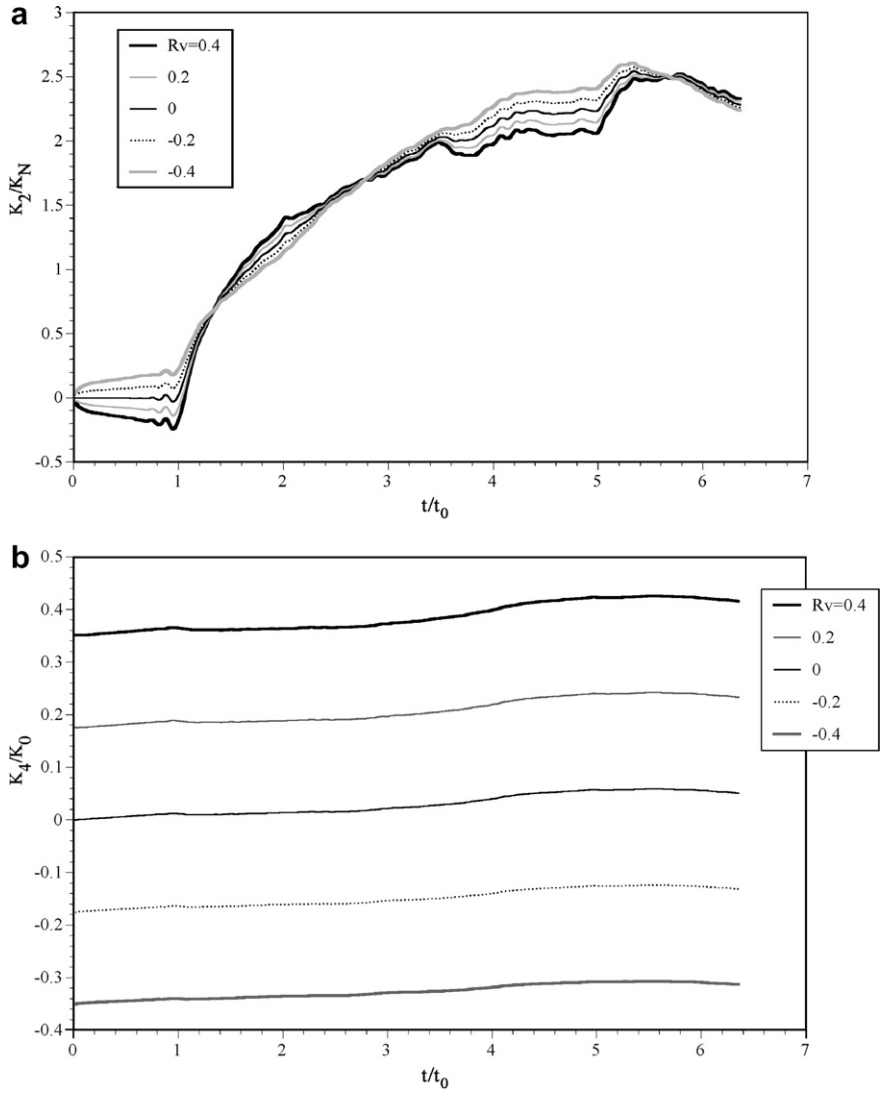

Fig. 18. Responses of the general dynamic SIFs in CdSe for Case 2: (a) the stress intensity factor K_2; (b) the electric displacement intensity factor K_4.

$$C_{sx} = \sqrt{(c_{33} + e_{13}^2/\kappa_{11})/\rho}, \quad C_{dx} = \sqrt{c_{11}/\rho}$$
$$C_{sy} = \sqrt{c_{33}/\rho}, \quad C_{dy} = \sqrt{(c_{22} + e_{22}^2/\kappa_{22})/\rho} \tag{25}$$

where C_{sx} and C_{dx} denote the shear and dilatational wave velocities propagating along the axis x_1, C_{sy} and C_{dy} denote the shear and dilatational wave velocities propagating along the axis x_2. Eq. (25) states that the piezoelectric effect makes the material stiffer, and induces larger wave velocities.

6.1. Impact response of a crack in PZT-4 plate

The impact responses of the dynamic J integral for PZT-4 are summarized in Fig. 7, which show the dynamic J integral for Case 1 and Case 2. Results are plotted for five values of electric displacement and electric field, but at the same mechanical load $\sigma_0 = 1.0$ kPa, where two dimensionless parameters are defined as

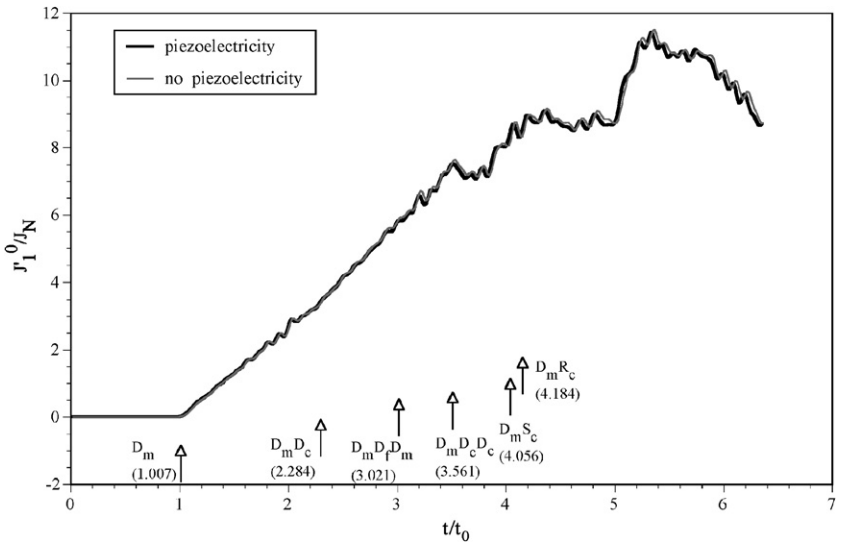

Fig. 19. The influence of piezoelectricity on the response of dynamic J integral in CdSe plate.

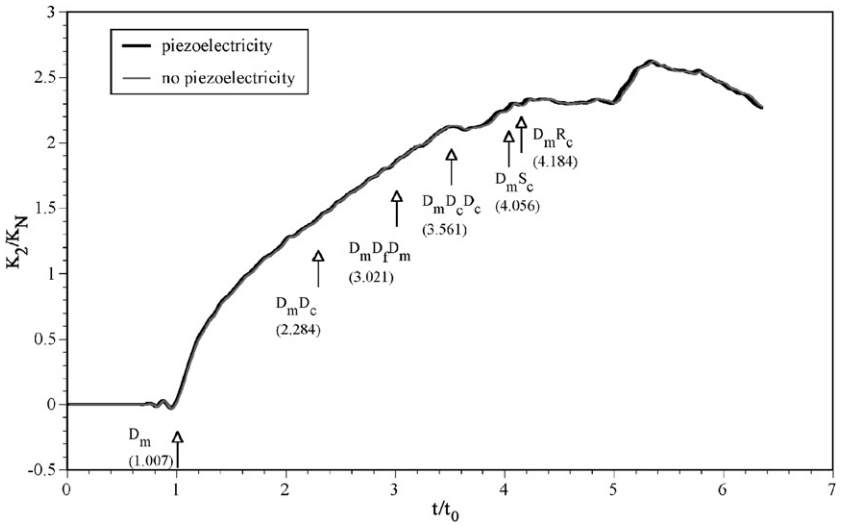

Fig. 20. The influence of piezoelectricity on the response of K_2 in CdSe plate.

$$R_{\mathrm{d}} = \frac{D_0 \times e_{22}}{\sigma_0 \times \kappa_{22}} \tag{26}$$

and

$$R_{\mathrm{v}} = \frac{E_0 \times e_{22}}{\sigma_0} \tag{27}$$

which denote the applied electric displacement and electric field, respectively. The applied electric field is computed as V/L (see Fig. 5(a)). The time-axis is normalized by $t_0 = L/C_{\mathrm{d}y}$, the dynamic J integral is normalized by $J_{\mathrm{N}} = \sigma_0^2 \pi a / c_{22}$. $t = 0$ is the time when the impact loading are applied to both upper and lower side of the plate.

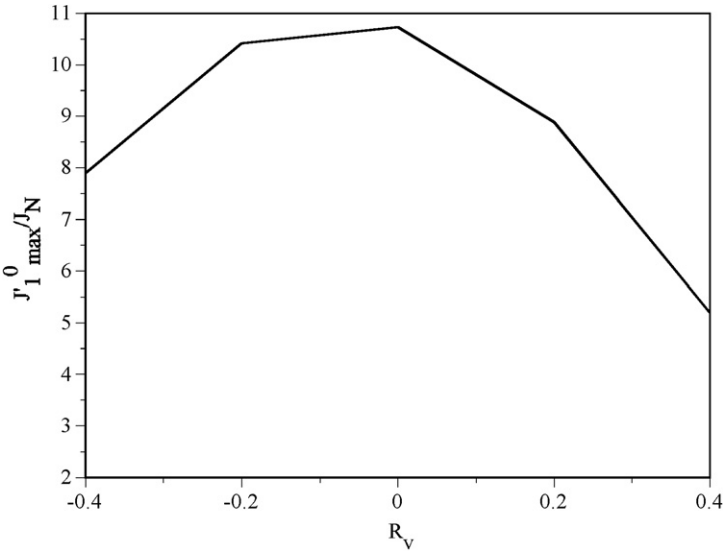

Fig. 21. Variation of the maximum values of dynamic J integral against R_{v} for CdSe plate.

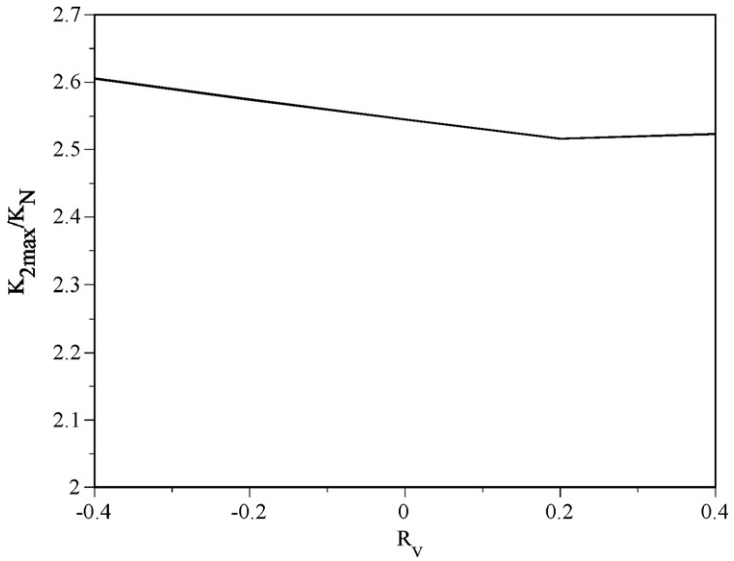

Fig. 22. Variation of the maximum values of K_2 against R_{v} for CdSe plate.

The corresponding stress and electric displacement intensity factors K_2 and K_4 are shown in Figs. 8 and 9 for Case 1 and 2, respectively. K_2 and K_4 are made dimensionless by divided by $K_N = \sigma_0(\pi a)^{1/2}$ and $K_0 = \sigma_0(\pi a)^{1/2}\kappa_{22}/e_{22}$, respectively. In contrast to the static problems, for dynamic problems the mechanical loading alone can produce electric displacement in the crack plane ahead of the crack tip and vice versa.

In Figs. 7(a) and 8(a), D_m is the time at which the front of the dilatational wave propagating along the x_2-axis reaches the crack tip. D_mD_c, D_mS_c and D_mR_c are the times when dilatational, shear and Rayleigh waves that radiate from the opposite crack tip, reach the crack tip in view. $D_mD_fD_m$ is the time at which the dilatational wave, reflected from the crack surface then re-reflected from the loading boarder, reach the crack tip. It is noted that we cannot capture the surface wave with the FEM, here we just show the moment in the figures when the waves arrive by theoritical calculation.

It can be seen that the impact response of dynamic J integral varying more wildly if the plate is subjected to electric loading. Before D_m, dynamic J integral varies very smoothly, and the positive electric field (or electric displacement) induces a negative K_2 while the negative one induces a positive K_2. After D_m, the incline of the response curve increases as the applied electric field increases. The response curve of K_2 comes to its maximum at the same time for the positive electric field (or electric displacement), while the negative electric loading seems to delay it. The oscillate amplitudes of the dynamic J integral, K_2 and K_4 increase as the applied electric field (or electric displacement) increases. Hence, the negative electric field (or electric displacement) impresses the oscillation while the positive one enforces it for piezoelectric material with strong electromechanical coupling factor. It is very interesting to find that the values of K_2 at $t/t_0 = 1.3$ are fixed when the electric displacement varies for Case 1 (see Fig. 8(a)). The same feature can be found in Fig. 9(a) for Case 2, where $t/t_0 = 1.58$. Before $t/t_0 = 1.58$ (or 1.3), K_2 decreases as the applied electric field increases while in some intervals after $t/t_0 = 1.58$ K_2 increases.

Figs. 10 and 11 depict the impact responses of the dynamic J integral and K_2, respectively, at the same mechanical load for PZT-4 plate with and without regards to piezoelectricity. The effect of piezoelectricity on the wave propagation is represented by the electromechanical coupling factor. For PZT-4, the electromechanical coupling factor, as aforementioned, is 0.5567 and is very high. Hence, the piezoelectricity affects the impact responses dramatically, and apparently the response curves seem to be totally different, as indicated in Figs. 10 and 11. Also marked in Figs. 10 and 11 are specific instants of time for the response curves without regards to piezoelectricity, which are much greater than those with regards to piezoelectricity (seen in Figs. 7(a) and 8(a)). It can be seen that the piezoelectricity induces larger wave velocities and decreases the

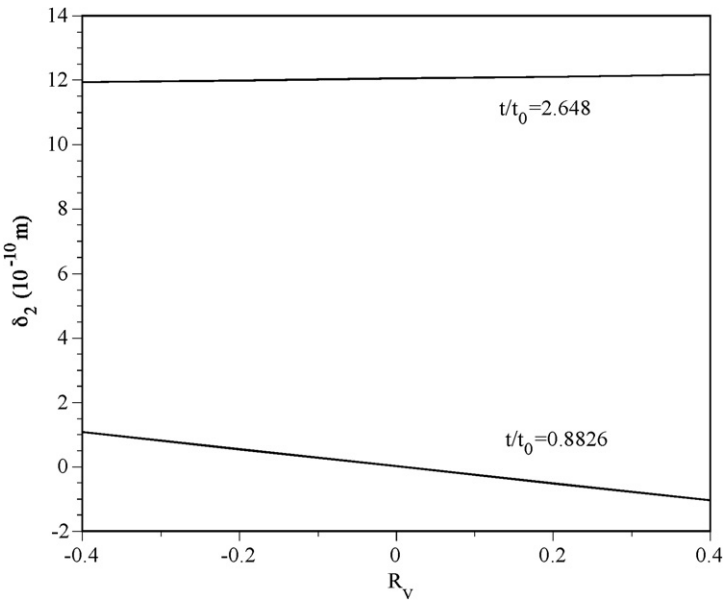

Fig. 23. Variation of the crack opening displacement δ_2 at distance $r = a/3$ behind the crack tip, against R_v for $t/t_0 = 0.8826$ and 2.648 in CdSe plate.

maximum values of response curves of dynamic J integral, but increases the maximum values of K_2 slightly. Without regards to piezoelectricity, PZT-4 is just an orthotropic material, and the impact response of J or K_2 goes to its maximum after time $D_m R_c$. This is different to that observed by Lin and Ballmann (1993) in isotropic material subject to an impact loading, where it comes to its maximum at time $D_m R_c$.

Figs. 12 and 13 plot the effect of the applied electric field on the maximum values of dynamic J integral and the corresponding stress intensity factor K_2, respectively. It can be seen that a positive electric field (or electric displacement) increases the maximum values of the dynamic J integral and K_2, while a negative one reduces them. These conclusions are in contrast to those for the static case for PZT-4: an applied electric field reduces the energy release rate whether the field is positive or negative, and the stress and electric displacement intensity factors are uncoupled (Park and Sun, 1995).

In Fig. 14, the relationships between the crack opening displacement δ_2, which is computed at distance $r = a/3$ behind the crack tip, and the applied electric field R_v are plotted for $t/t_0 = 0.8826$ and 2.648. It can be found that the crack opening displacement decreases with the increase of an applied electric field at $t/t_0 = 0.8826$, which means that the positive electric field makes the crack close together before the dilatational wave reaches the crack line. For a macro-crack, this value is so small that it cannot make the crack surfaces contact together. This is also the reason why the negative K_2 before D_m is permitted in this paper. At

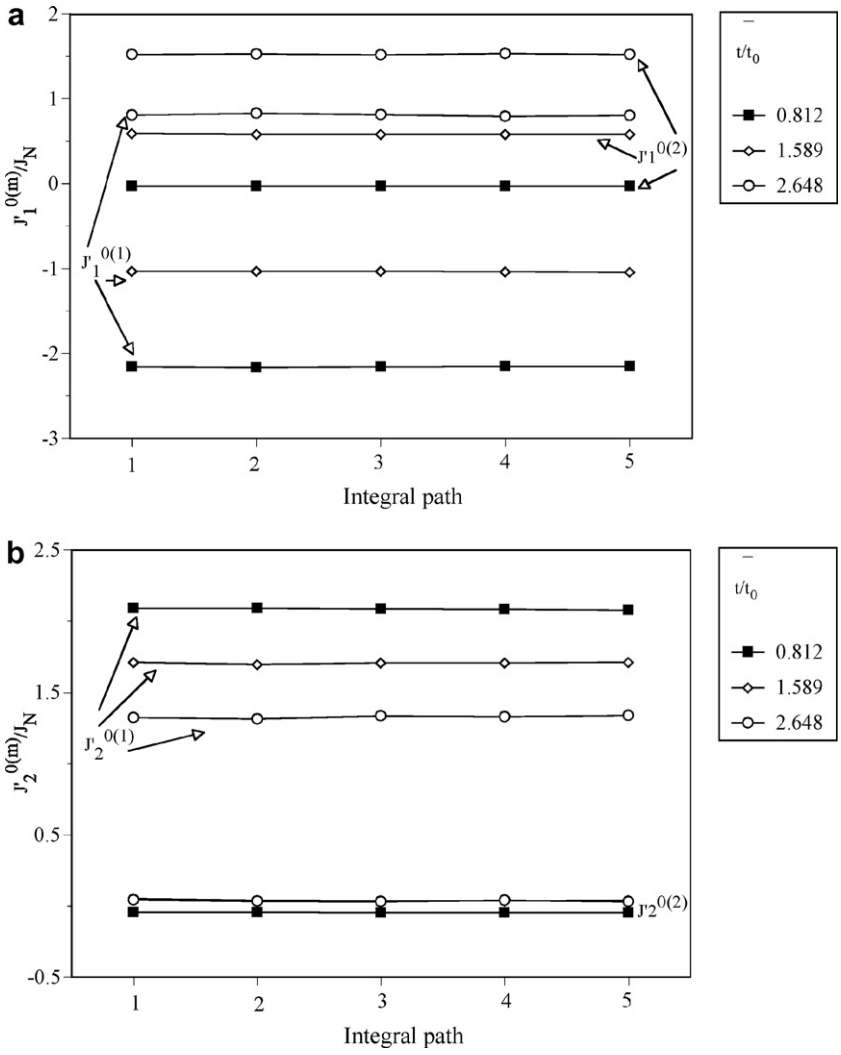

Fig. 24. Path independence of separated dynamic J integrals at $R_v = 0.2$ in CdSe/PZT-4 bimaterial plate: (a) J_1^{*0}; (b) J_2^{*0}.

$t/t_0 = 2.648$, the crack opening displacement increases with the increase of the applied electric field, which means that the positive electric field makes the crack open after the dilatational wave reaches the crack line.

The separated dynamic J integrals can also be applied to a homogeneous model. Imagining that there is an interface at the center of the plate along the crack, then simulate the model (see Fig. 5) as if it is a bimaterial plate though the material properties of both upper and lower part of the plate are identical. The impact response of the separated dynamic J integrals for $R_v = 0.4$ is shown in Fig. 15. It is seen that the separated dynamic J are identical with each other in the whole period of simulation, and their sum is equal to the dynamic J integral for such a crack in homogeneous plate.

6.2. Impact response of a crack in CdSe plate

Due to the lower electromechanical coupling factor, the impact dynamic responses of CdSe are very different from those of PZT-4, and somewhat similar to those for static problems. The impact responses of the

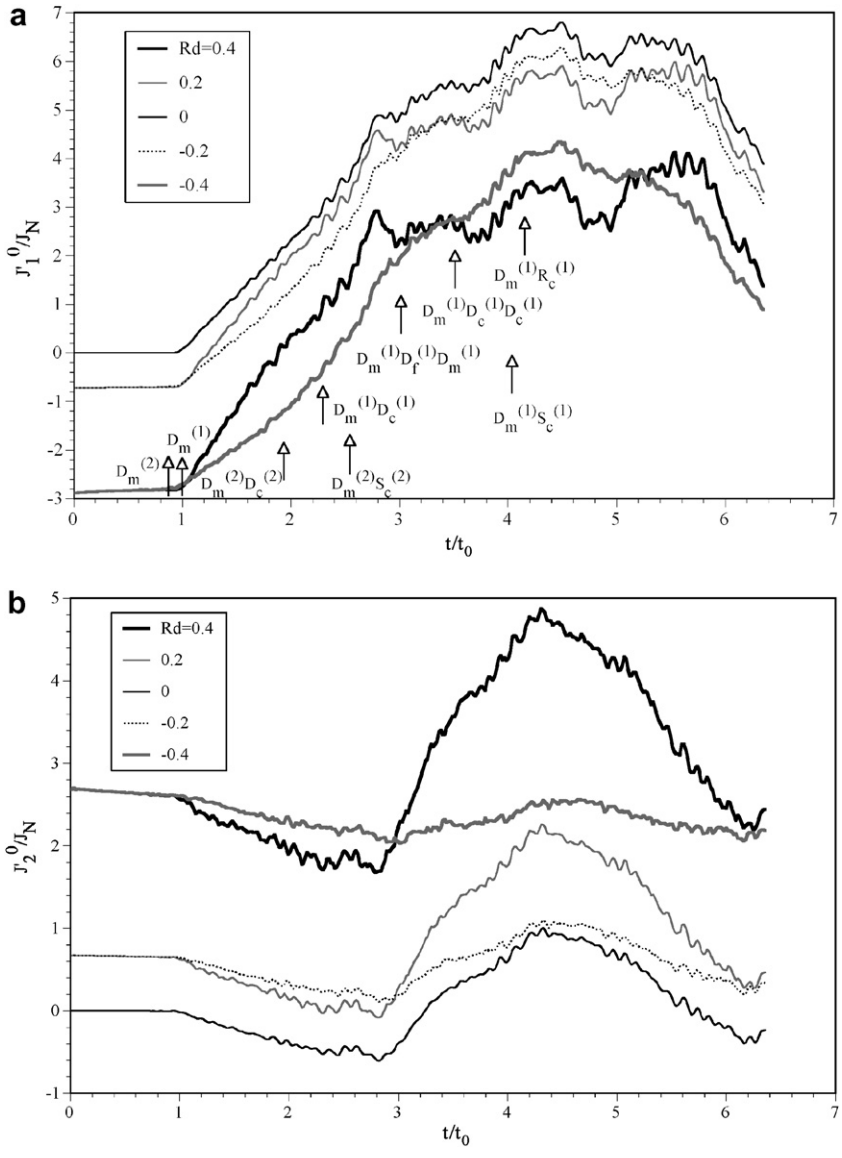

Fig. 25. Dynamic J integral response in CdSe/PZT-4 bimaterial plate for Case 1: (a) J_1^0; (b) J_2^0.

dynamic J integral for CdSe are presented in Fig. 16. Results are also plotted for five values of electric displacement and electric field, but at the same mechanical load $\sigma_0 = 1.0$ kPa. In this section, the normalization is same as that in Section 6.1, but it should be borne in mind that the material parameters and wave velocities of CdSe are used in this section.

The corresponding stress and electric displacement intensity factors K_2 and K_4 are plotted in Figs. 17 and 18 for Case 1 and 2, respectively. Although the mechanical loading alone can also produce electric displacement in the crack plane ahead of the crack tip and vice versa, comparing to PZT-4, the amplitudes of the variation of K_4 are much smaller. In fact K_4 almost keeps a constant, that is due to the weak electromechanical coupling factor.

From Fig. 16, it can be seen that an applied electric field (or electric displacement) reduces dynamic J integral (energy release rate) whether the field (or electric displacement) is positive or negative. At the same magnitude, a positive electric field has somewhat bigger effect than a negative one. This conclusion, in contrast to that for PZT-4, is same as that for the static problem (see Park and Sun, 1995; McMeeking, 1999). Similar to PZT-4, before D_m, dynamic J integral varies very smoothly, and an applied positive electric field (or electric

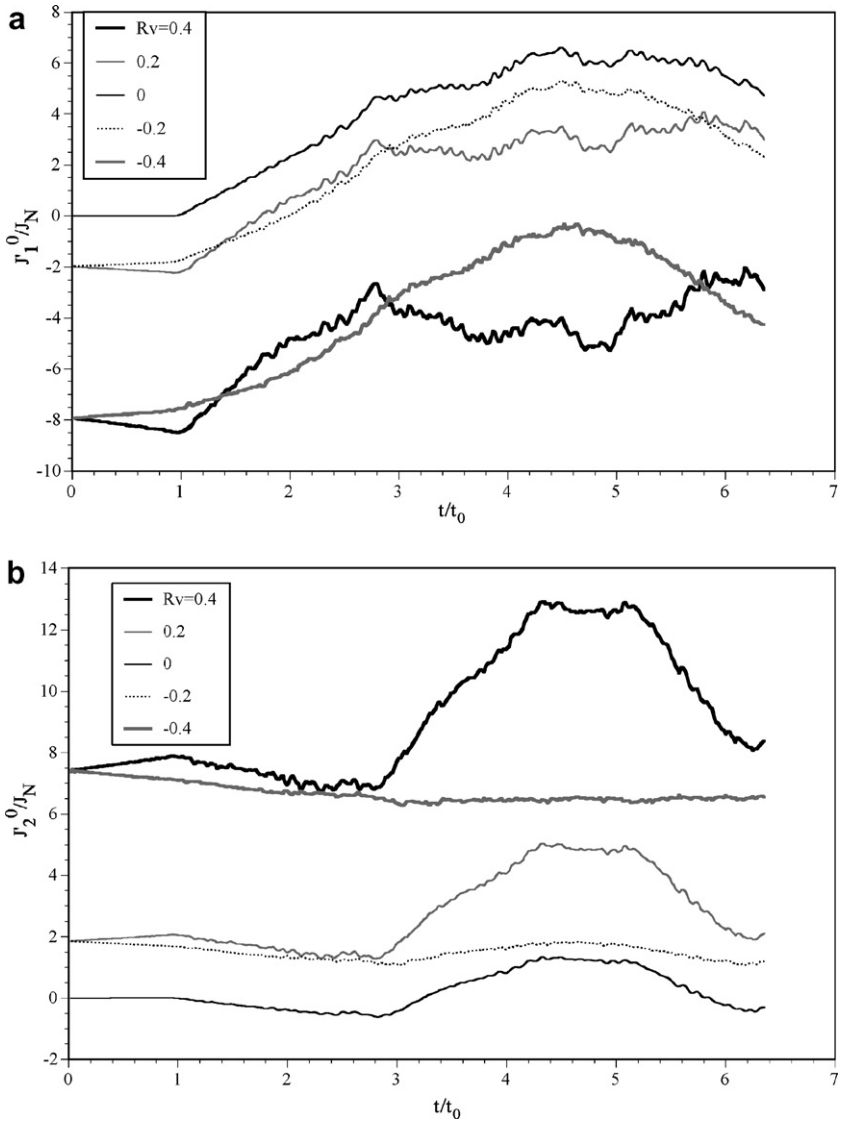

Fig. 26. Dynamic J integral response in CdSe/PZT-4 bimaterial plate for Case 2: (a) $J_1^{/0}$; (b) $J_2^{/0}$.

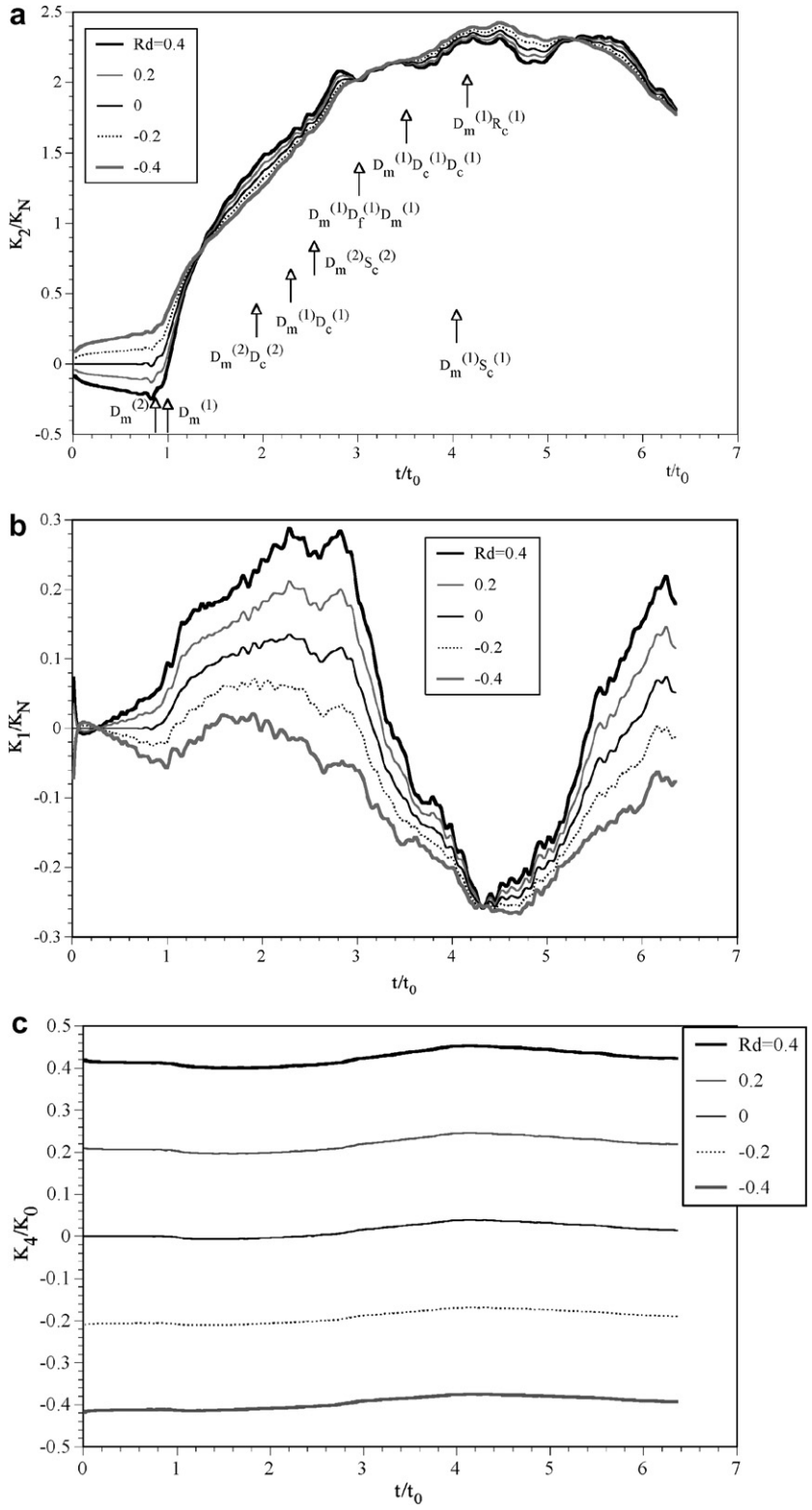

Fig. 27. Responses of the general dynamic stress intensity factors in CdSe/PZT-4 plate for Case 1: (a) K_2; (b) K_1; (c) K_4.

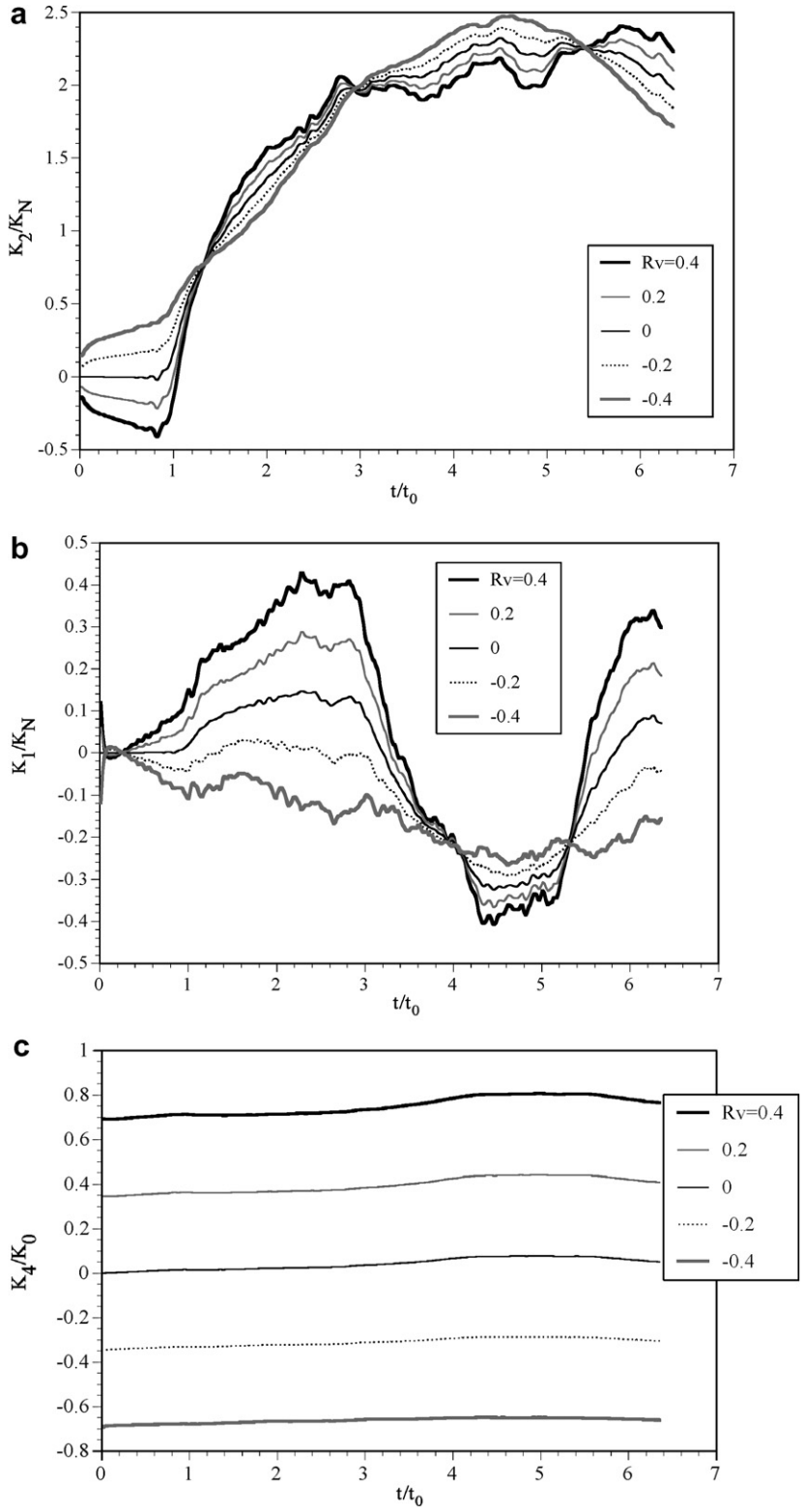

Fig. 28. Responses of the general dynamic stress intensity factors in CdSe/PZT-4 plate for Case 2: (a) K_2; (b) K_1; (c) K_4.

displacement) induces a negative K_2 while the negative one induces a positive K_2. The response curve of K_2 comes to its maximum at the same time, which does not depend on R_v or R_d. Figs. 17(a) and 18(a) show that the electric loading affects K_2 very slightly. For piezoelectric material with weak electromechanical coupling factor, it cannot reach the conclusions that the negative electric field (or electric displacement) impresses the oscillation while the positive one enforces it. It is also noted that the value of the stress intensity factor K_2 keeps constant at $t/t_0 = 1.32$ as an electric displacement varies for Case 1 (see Fig. 17(a)), and so does it at $t/t_0 = 1.38$ as an applied electric field changes for Case 2 (see Fig. 18(a)).

Figs. 19 and 20 show the impact responses of the dynamic J integral and K_2, respectively, at the same mechanical load for CdSe plate with and without regards to piezoelectricity. For CdSe, the electromechanical coupling factor is small, as aforementioned. Specific instants of time are also marked in Figs. 19 and 20 for those without regards to piezoelectricity, which are little greater than those with regards to piezoelectricity (see in Figs. 16(a) and 17(a)). It can be seen that the piezoelectricity has little effect on the impact response curves of dynamic J integrals and K_2, that even can be omitted. Similar to PZT-4, the impact responses of J and K_2 go to their maximum after time $D_m R_c$.

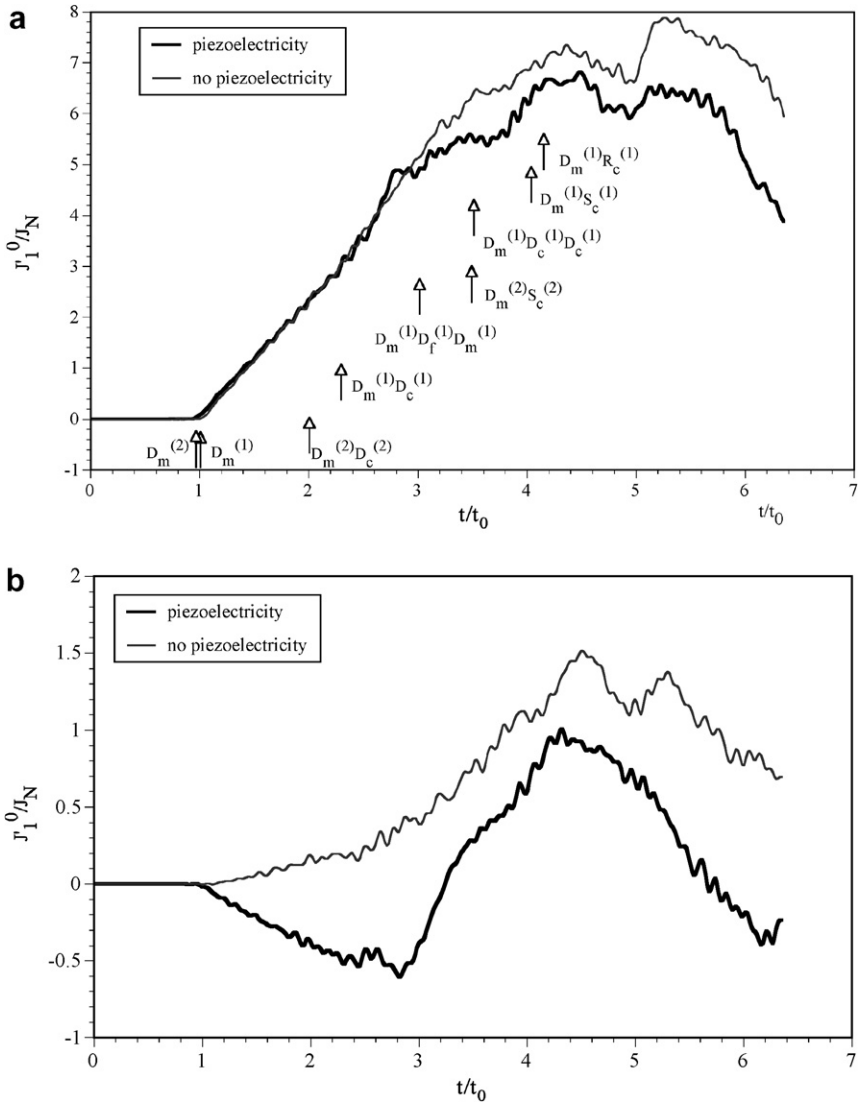

Fig. 29. The influence of piezoelectricity on the response of dynamic J integrals in CdSe/PZT-4 plate: (a) $J_1^{'0}$; (b) $J_2^{'0}$.

The effects of the applied electric field on the maximum values of response curves of dynamic J integral and the corresponding stress intensity factor K_2 are plotted in Figs. 21 and 22, respectively. It can be seen that an applied electric field (or electric displacement) reduces the maximum values of response curves of dynamic J integral (energy release rate) whether the field (or electric displacement) is positive or negative. At the same magnitude, a positive electric field has somewhat bigger effect than a negative one. These conclusions are consistent to those for the static problems (Park and Sun, 1995). For Case 1, an applied electric displacement has no effect on the maximum values of impact response curves of dynamic K_2; for Case 2, a positive electric field decreases the maximum values of impact response curves of dynamic K_2 while a negative one increases it. However, the variation is very limited, as shown in Fig. 22.

The relations between the crack opening displacement δ_2, which is also computed at distance $r = a/3$ behind the crack tip, and the applied electric field R_v are plotted in Fig. 23 for $t/t_0 = 0.8826$ and 2.648. Similar to PZT-4, it can be found that the crack opening displacement decreases with the increase of an applied electric field before D_m (at $t/t_0 = 0.8826$). After D_m (at $t/t_0 = 2.648$), the crack opening displacement increases with the increase of an applied electric field. However, different from PZT-4, the increment of

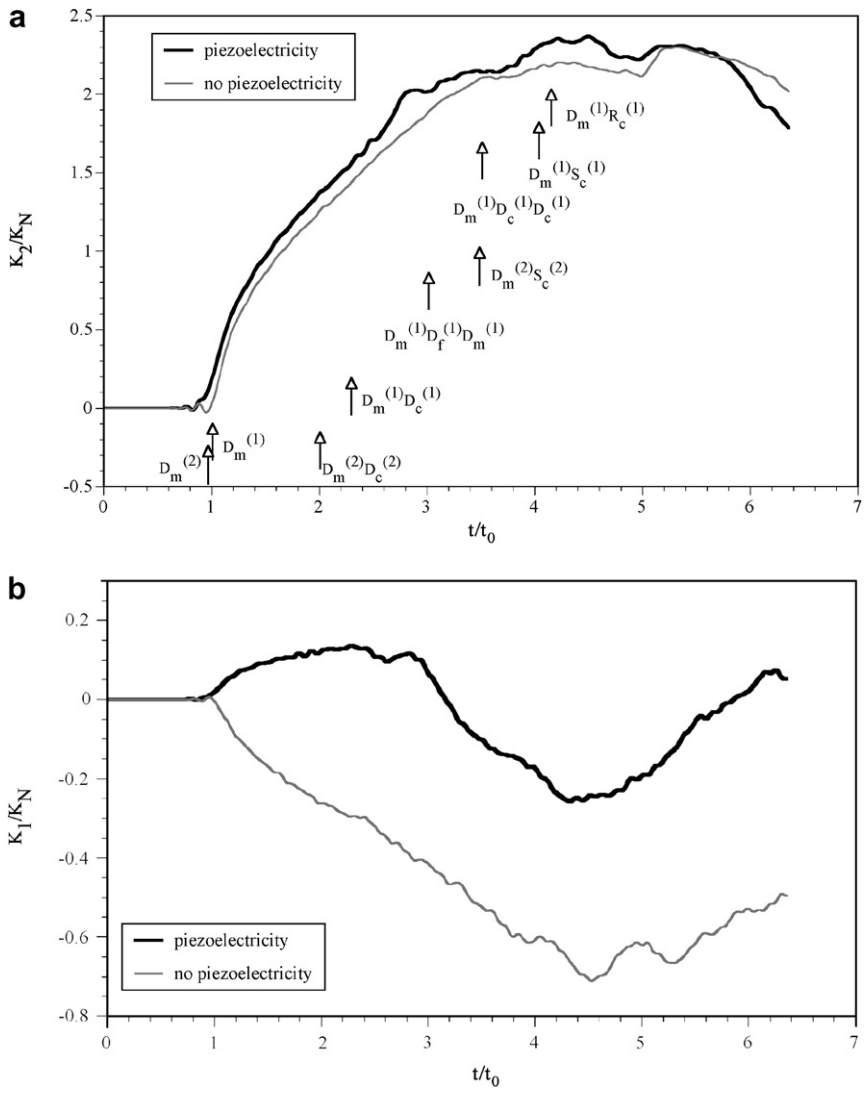

Fig. 30. The influence of piezoelectricity on the response of K_2 in CdSe/PZT-4 plate: (a) K_2; (b) K_4.

the crack opening displacement is very small, the effect of the applied electric field on the crack opening displacement is very slight.

The impact response of the separated dynamic J integral for the condition of $R_v = 0.2$ is also calculated. Similar to PZT-4, the separated dynamic J are identical with each other in the whole period of simulation, and their sum is equal to the dynamic J integral. The results are omitted here.

7. Impact response of an interfacial crack

A bimaterial system composed of CdSe and PZT-4 with a center crack is considered in this section (see Fig. 5). CdSe, the more compliant part of the bimaterial system, is named material 1 and placed at upper side, while PZT-4, the stiffer one, is named material 2 and placed at lower side of the interface. The plate is subjected to impact mechanical/electric loading of step function type at time $t = 0$. Similar to Section 5, the electric loading is electric displacement (Case 1) or electric potential (Case 2), as shown in Fig. 5. The dimensions of the plate are identical with those in homogeneous model.

In this section, two dimensionless parameters are defined as

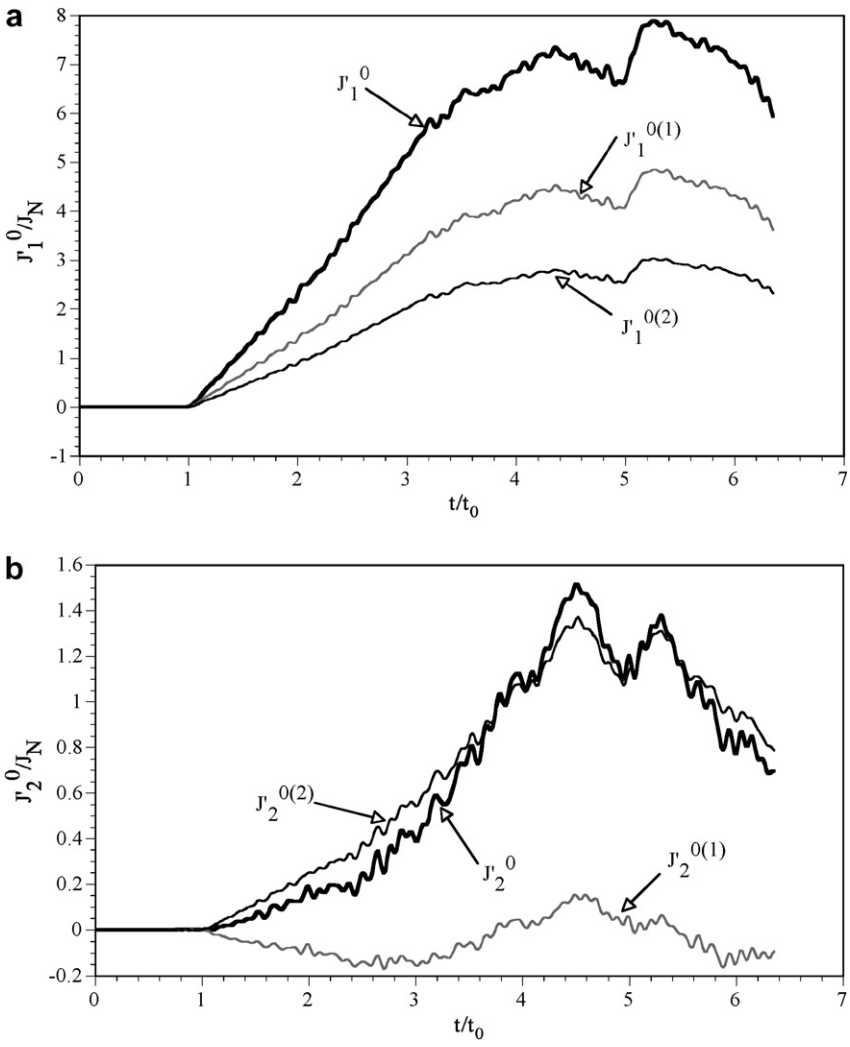

Fig. 31. Responses of separated dynamic J integrals in CdSe/PZT-4 plate without regards to piezoelectricity: (a) J_1^{*0}; (b) J_2^{*0}.

$$R_{\mathrm{d}} = \frac{D_0 \times e_{22}^{(1)}}{\sigma_0 \times \kappa_{22}^{(1)}} \tag{28}$$

and

$$R_{\mathrm{v}} = \frac{E_0 \times e_{22}^{(1)}}{\sigma_0} \tag{29}$$

which denote the impact applied electric displacement and electric field, respectively. The superscript (m) denotes the material m. In these simulations, the impact step mechanical load σ_0 keeps to be 1.0 kPa, for electric loading, R_{v} and R_{d} are taken to be -0.4, -0.2, 0, 0.2 and 0.4. The time-axis is normalized by $t_0 = L/C_{\mathrm{d}y}^{(1)}$, the dynamic J integral is normalized by $J_{\mathrm{N}} = \sigma_0^2 \pi a / c_{22}^{(1)}$. $t = 0$ is the time when the impact loading are applied to both upper and lower side of the plate.

The separated dynamic J integrals are evaluated by Eq. (23) for five circular integral paths (see Fig. 6). Fig. 24 indicates excellent path independence of the separated dynamic J integrals, for Case 2 at $R_{\mathrm{v}} = 0.2$.

The impact responses of the dynamic J integrals are shown in Figs. 25 and 26, which show the dynamic J integrals for Case 1 and Case 2, respectively. The corresponding stress and electric displacement intensity

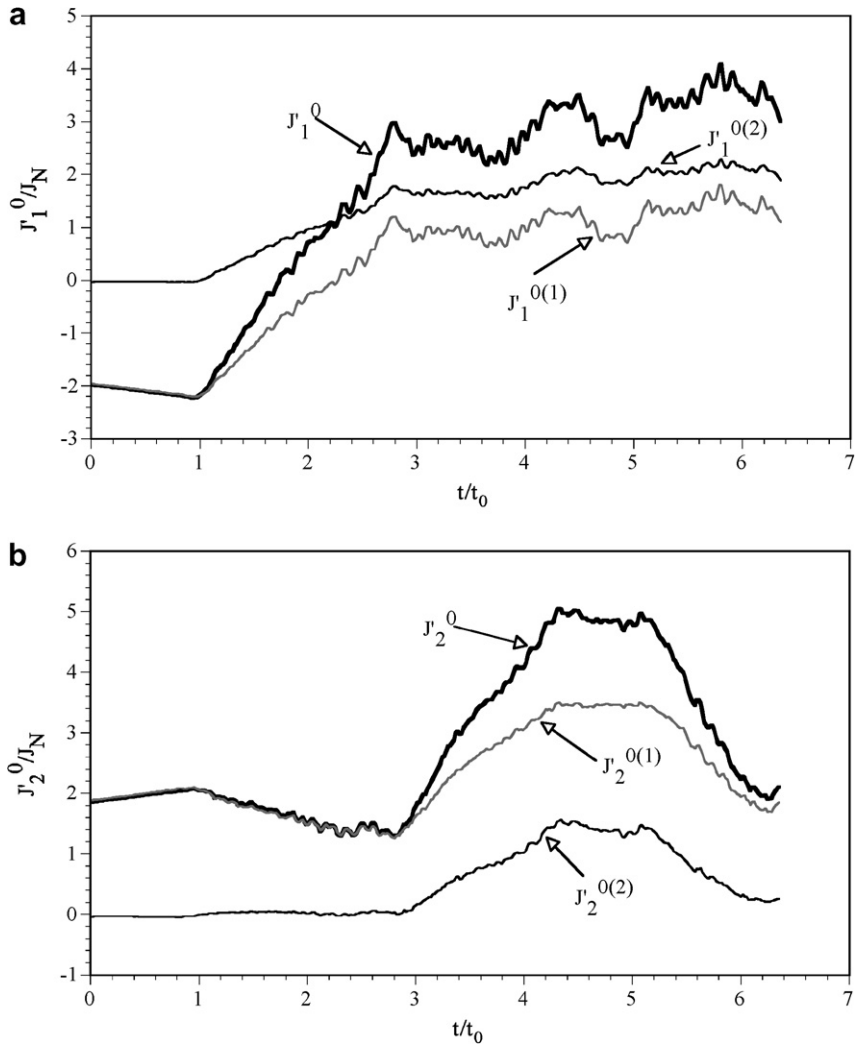

Fig. 32. Responses of separated dynamic J integrals at $R_{\mathrm{v}} = 0.2$ in CdSe/PZT-4 plate: (a) $J_1'^0$; (b) $J_2'^0$.

factors K_2, K_1 and K_4 are shown in Figs. 27 and 28 for Case 1 and 2, respectively. K_2, K_1 and K_4 are made dimensionless by divided by $K_N = \sigma_0(\pi a)^{1/2}$ and $K_0 = \sigma_0(\pi a)^{1/2}\kappa_{22}^{(1)}/e_{22}^{(1)}$, respectively. The amplitudes of the variation of K_4 are so small that K_4 almost keeps a constant.

In Figs. 25(a) and 27(a), $D_m^{(1)}$ and $D_m^{(2)}$ is the time when the lower and higher dilatational waves propagating along the x_2-axis impinge to the crack tip line, respectively (here, the lower wave velocity is of material 1, and the higher one is of material 2). $D_m^{(1)}D_c^{(1)}$, $D_m^{(1)}S_c^{(1)}$ and $D_m^{(1)}R_c^{(1)}$ are the times when the lower dilatational, shear and Rayleigh waves that radiate from the opposite crack tip, reaches the crack tip of interest. $D_m^{(1)}D_f^{(1)}D_m^{(1)}$ is the time at which the lower dilatational wave, reflected from the crack surface then re-reflected from the loading boarder, reaches the crack tip. It can be seen that the impact response of dynamic J integral varying more wildly if the plate is subjected to applied electric field. From Figs. 25 and 27, it can be seen that an applied electric field (or electric displacement) reduces dynamic $J_1'^0$ integral (energy release rate) and increases dynamic $J_2'^0$ integral whether the field (or electric displacement) is positive or negative. At the same magnitude, a positive electric field has somewhat bigger effect than a negative one. The oscillate amplitudes of the dynamic $J_2'^0$ integral and K_1 increase as the applied electric field (or electric displacement) increases. Hence, the negative electric field (or electric displacement) impresses the anti-plane oscillation while the positive one enforces it for CdSe/PZT-4 bimaterial. Before the lower dilatational stress wave reaches the crack tip line ($D_m^{(1)}$), the dynamic J integral varies very smoothly, and the positive electric field (or electric displacement) induces a negative K_2 while the negative one induces a positive K_2. After $D_m^{(1)}$, at the same magnitude, a positive electric field (or electric displacement) induces a bigger incline of the response curve of dynamic $J_1'^0$ integral than a negative one. The response curves of $J_1'^0$ and K_2 come to their maximum later for a positive electric field (or electric displacement). It is also noted that K_2 at $t/t_0 = 1.31$ keeps a constant value as the electric displacement changes for Case 1 (see Fig. 27(a)). The same feature can be found in Fig. 28(a) for Case 2, where $t/t_0 = 1.32$. Before $t/t_0 = 1.32$ (or 1.31), the stress intensity factor K_I decreases as the applied electric field increases while in some intervals after $t/t_0 = 1.32$ K_I increases.

Figs. 29 and 30 show the impact responses of the dynamic J integral and K_2, K_1 respectively, at the same mechanical load for CdSe/PZT-4 bimaterial plate with and without regards to piezoelectricity. Specific instants of time are also marked in Figs. 29 and 30 for these without regards to piezoelectricity. It can be seen that the piezoelectricity reduces dynamic J integrals, while it increases the stress intensity factor K_2 and K_1. The piezoelectricity makes the response curves of $J_1'^0$ and K_2 to come to their maximum earlier.

Without regards to piezoelectricity, the response curves of the separated dynamic J integrals are shown in Fig. 31. It is seen that the separated dynamic J integral or equivalently the separated energy release rate of the

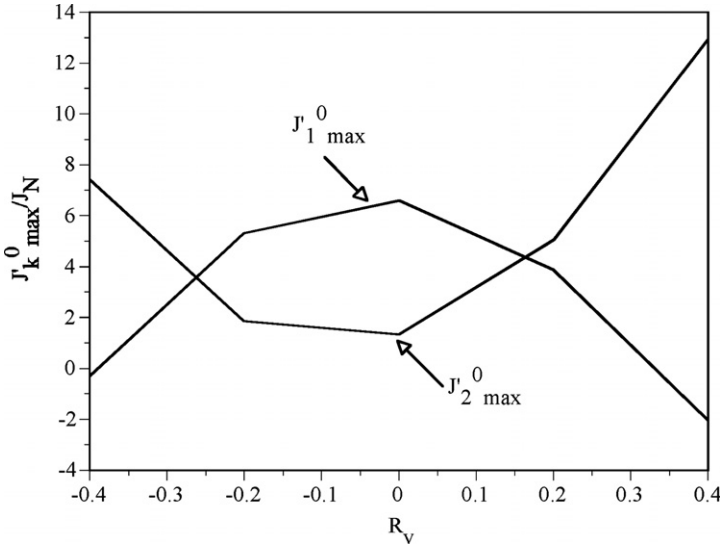

Fig. 33. Variation of the maximum values of dynamic J integrals against R_v for CdSe/PZT-4 plate.

compliant material side $J_1'^{0(1)}$ is larger than that of the stiff material side $J_1'^{0(2)}$. This observation is same as that for the isotropic bimaterial (Nishioka and Yasin, 1999). With regards to piezoelectricity, the impact response of the separated dynamic J integral for the condition of $R_v = 0.2$ is also shown in Fig. 32. It is seen that the oscillate amplitudes of the dynamic J integral of the compliant material side $J_1'^{0(1)}$ is much larger than that of the stiff material side $J_1'^{0(2)}$.

The effect of the applied electric field on the maximum values of dynamic J integral and the corresponding K_2 and K_1, are plotted in Figs. 33 and 34, respectively. It can be seen that an applied electric field (or electric displacement) reduces the maximum values of $J_1'^0$ and increases the maximum values of $J_2'^0$ whether the field is positive or negative. At the same magnitude, a positive electric field has somewhat bigger effect than a negative one. K_1 increases monotonously with the increase of an applied electric field. A negative applied electric field increases the maximum values of K_2, while a positive electric field has somewhat weaker effect than a negative one although it postpones the time when K_2 goes to its maximum.

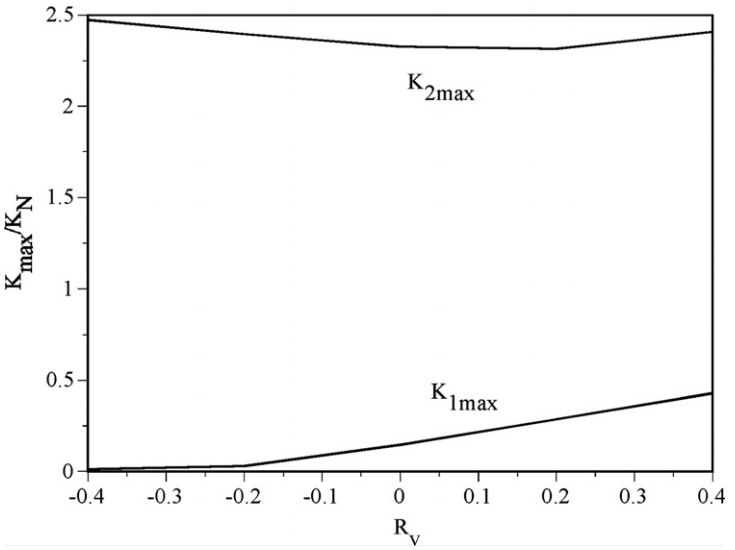

Fig. 34. Variation of the maximum values of K_2 and K_1 against R_v for CdSe/PZT-4 plate.

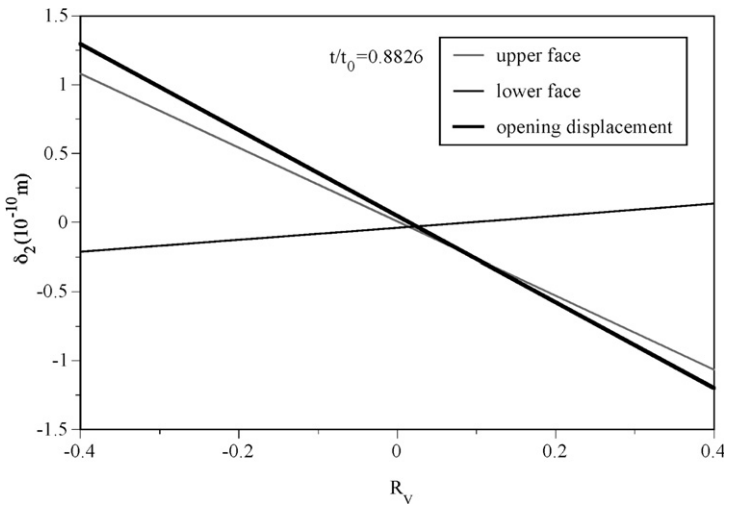

Fig. 35. Variation of the crack opening displacement δ_2 at distance $r = a/3$ behind the crack tip, against R_v for $t/t_0 = 0.8826$ in CdSe/PZT-4 plate.

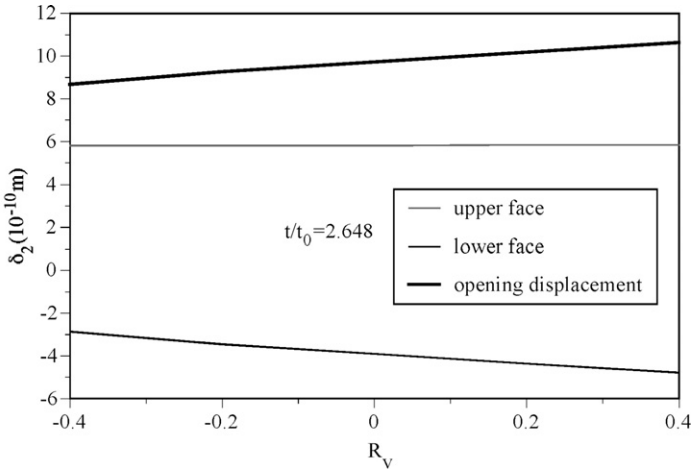

Fig. 36. Variation of the crack opening displacement δ_2 at distance $r = a/3$ behind the crack tip, against R_v for $t/t_0 = 2.648$ in CdSe/PZT-4 plate.

Figs. 35 and 36 show displacements of the upper and lower faces of the crack, as well as the crack opening displacement δ_2, which are computed at distance $r = a/3$ behind the crack tip, against the applied electric field R_v for $t/t_0 = 0.8826$ and 2.648, respectively. The crack opening displacement, the displacements of the upper and lower surfaces of the interfacial crack decreases with the increase of an applied electric field at $t/t_0 = 0.8826$. This means that the positive electric field makes the interfacial crack close together before the lower dilatational wave reaches the crack line. At $t/t_0 = 2.648$, the crack opening displacement, the displacements of the upper and lower surfaces of the interfacial crack increases with the increase of the applied electric field, which means that the positive electric field makes the crack open after the lower dilatational wave reaches the crack line. The effect of the applied electric field on the deformations of the lower electromechanical coupling material (CdSe) is very slight, and the displacement of the upper surface of the interfacial crack is almost independent of R_v. From these 2 figures, it can be seen that the deformations of the compliant material (CdSe) are larger than those of the stiff material (PZT-4).

8. Conclusions

In this paper, simulations of a stationary crack in both homogeneous and bimaterial subject to an electromechanical impact loading are carried out. The path-independence of separated dynamic J integrals is confirmed from the numerical simulations. In this dynamic finite element analysis, the component separation method of the dynamic J integrals is used to calculate the mixed-mode stress and electric displacement intensity factors. The response curves of the dynamic J integrals and the stress and electric displacement intensity factors are obtained for both homogeneous material and bimaterial. In homogeneous material, in contrast to the static problems, the impact mechanical loading alone can produce electric displacement in the crack plane ahead of the crack tip and vice versa. The piezoelectricity makes the material harder, and induces larger wave velocities. The influence of piezoelectricity on the wave propagation is represented by the electromechanical coupling factor. The influence of the piezoelectricity on the impact responses is strong for piezoelectric materials with high electromechanical coupling factor, while it is weak for those with low electromechanical coupling factor. For bimaterial, the oscillate amplitudes of the dynamic J integral of the compliant material side $J_1^{\prime 0(1)}$ is much larger than that of the stiff material side $J_1^{\prime 0(2)}$, so is the deformation. The effects of an applied electric field on the impact responses depend on the electromechanical coupling factor.

The results also indicate that the piezoelectric material with high electromechanical coupling factor, such as PZT-4, is a good choice to control the deformation (or the vibration) and be used as actuator, because an applied electric field affects the deformation and stress fields strongly. In contrast, the piezoelectric material with low electromechanical coupling factor, such as CdSe, can be used as sensor in non-destructive techniques

and other applications, because an applied electric field produces an electric wave for detection with little effect on the deformation and stress fields and the elastic wave propagation.

Acknowledgements

We appreciate supports from NSFC (Grant No. 10672130), Ministry of Education of China (Program for NCET in University), 973 Program (2007CB707702), and JSPS program.

Appendix A

Consider a Cartesian coordinate (x_1, x_2, x_3) with origin at the middle of the interfacial crack between two bonded dissimilar, anisotropic piezoelectric solids. The x_3-axis is in the out of paper direction. The x_1-axis is directed along the line of the crack and x_2-axis along the direction of the perpendicular bisector of the crack. The generalized two-dimensional deformation is considered in which the three components of displacement and the electric potential depend only on in-plane coordinates. Suppose that the crack is moving with constant velocity v in the x_1 direction. After sufficient time, a steady state will be attained.

The constitutive equation for either one of the two anisotropic piezoelectric materials can be written as

$$\begin{aligned}\sigma_{ij} &= C_{ijrs}u_{r,s} + e_{sji}\varphi_{,s}\\ D_i &= -\varepsilon_{is}\varphi_{,s} + e_{irs}u_{r,s}\end{aligned} \tag{A.1}$$

where C_{ijrs}, e_{sji} and ε_{is} are the elasticity constants, piezoelectricity constants and permittivity constants, respectively. u_i is mechanical displacement, σ_{ij} mechanical stress tensor, φ and D_i are potential and the induction of the electrical field. In this paper, for convenience, the subscripts I, II are used to designate the upper and lower materials, which will be dropped unless it is necessary to distinguish the upper and lower half-spaces. The repeated indices imply summation. The displacements and stresses will be of the form

$$u_i = u_i(x_1 - vt, x_2) \quad \sigma_{ij} = \sigma_{ij}(x_1 - vt, x_2)$$

The dynamic governing equations for piezoelectric materials are

$$\begin{aligned}&(c_{ijrs}u_r + e_{sji}\varphi)_{,si} = \rho\frac{\partial^2 u_j}{\partial t^2}\\ &(-\varepsilon_{is}\varphi + e_{irs}u_r)_{,si} = 0\end{aligned} \tag{A.2}$$

where ρ is density. It is notable that the body force other than inertia and the free charge are not considered in the present work.

Denoting

$$\mathbf{U} = [\,u_1 \quad u_2 \quad u_3 \quad \varphi\,]^{\mathrm{T}} \quad \mathbf{t} = [\,\sigma_{21} \quad \sigma_{22} \quad \sigma_{23} \quad D_2\,]^{\mathrm{T}} \quad \mathbf{s} = [\,\sigma_{11} \quad \sigma_{12} \quad \sigma_{13} \quad D_1\,]^{\mathrm{T}}$$

(A.2) can be rewritten as

$$\mathbf{Q}_1\mathbf{U}_{,11}(x_1, x_2, t) + (\mathbf{R} + \mathbf{R}^{\mathrm{T}})\mathbf{U}_{,12}(x_1, x_2, t) + \mathbf{W}\mathbf{U}_{,22}(x_1, x_2, t) = \rho\frac{\partial^2 \mathbf{U}(x_1, x_2, t)}{\partial t^2} \tag{A.3}$$

where

$$\mathbf{Q}_1 = \begin{bmatrix}\mathbf{Q}_0 & \mathbf{e}_{11}\\ \mathbf{e}_{11}^{\mathrm{T}} & -\varepsilon_{11}\end{bmatrix}, \quad \mathbf{R} = \begin{bmatrix}\mathbf{R}_0 & \mathbf{e}_{21}\\ \mathbf{e}_{12}^{\mathrm{T}} & -\varepsilon_{12}\end{bmatrix}, \quad \mathbf{W} = \begin{bmatrix}\mathbf{W}_0 & \mathbf{e}_{22}\\ \mathbf{e}_{22}^{\mathrm{T}} & -\varepsilon_{22}\end{bmatrix}$$

with

$$\begin{aligned}&(\mathbf{Q}_0)_{ik} = c_{i1k1}, \quad (\mathbf{R}_0)_{ik} = c_{i1k2}, \quad (\mathbf{W}_0)_{ik} = c_{i2k2} \qquad (i,k = 1,2,3)\\ &\mathbf{e}_{ik} = [\,e_{i1k} \quad e_{i2k} \quad e_{i3k}\,]^{\mathrm{T}}, \qquad (i,k = 1,2)\end{aligned}$$

For convenience, we introduce $\mathbf{L} = \mathrm{diag}[\,1 \quad 1 \quad 1 \quad 0\,]$. From the constitutive relations, we have

$$\mathbf{t} = \mathbf{R}^{\mathrm{T}}\mathbf{U}_{,1} + \mathbf{W}\mathbf{U}_{,2} \quad \mathbf{s} = \mathbf{Q}_1\mathbf{U}_{,1} + \mathbf{R}\mathbf{U}_{,2} \tag{A.4}$$

By introducing the moving coordinate $(\eta_1, \eta_2) = (x_1 - vt, x_2)$, (A.3) became

$$\mathbf{Q}\mathbf{U}_{,11} + (\mathbf{R} + \mathbf{R}^{\mathrm{T}})\mathbf{U}_{,12} + \mathbf{W}\mathbf{U}_{,22} = 0 \tag{A.5}$$

where

$$\mathbf{Q}(v) = \mathbf{Q}_1 - \rho v^2\mathbf{L}$$

In general, the extended displacements and stresses can be represented

$$\mathbf{u} = \mathbf{A}\mathbf{f}(z) + \bar{\mathbf{A}}\bar{f}(z) \tag{A.6}$$

$$\mathbf{t} = \mathbf{B}\mathbf{f}'(z) + \bar{\mathbf{B}}\bar{f}'(z) \tag{A.7}$$

where $\mathbf{A} = [\,\mathbf{a}_1 \quad \mathbf{a}_2 \quad \mathbf{a}_3 \quad \mathbf{a}_4\,], \mathbf{B} = [\,\mathbf{b}_1 \quad \mathbf{b}_2 \quad \mathbf{b}_3 \quad \mathbf{b}_4\,]$. In the above, $z_\alpha = \eta_1 + p_\alpha\eta_2$, $\mathbf{a}_\alpha$, p_α are determined by the following eigen equations (Shen and Kuang, 1998)

$$\mathbf{J}(p)\mathbf{a} = [\mathbf{Q} + (\mathbf{R} + \mathbf{R}^{\mathrm{T}})p + \mathbf{W}p^2]\mathbf{a} = 0 \tag{A.8}$$

To determine the eigenvalue p_α, from (8) we have

$$\|(\mathbf{Q}_1 - \rho v^2\mathbf{I}) + (\mathbf{R} + \mathbf{R}^{\mathrm{T}})p + \mathbf{W}p^2\| = 0 \tag{A.9}$$

Eq. (A.9) has eight roots which cannot be real. The eight roots form four conjugate pairs and we shall choose $\mathbf{Im}(p_\alpha) > 0$ for $\alpha = 1,2,3,4$. The matrix $\mathbf{A}$ and $\mathbf{B}$ have the following correlation

$$\mathbf{b}_\alpha = (\mathbf{R}^{\mathrm{T}} + p_\alpha\mathbf{W})\mathbf{a}_\alpha = -\frac{1}{p_\alpha}(\mathbf{Q} + p_\alpha\mathbf{R})\mathbf{a}_\alpha \tag{A.10}$$

The matrix $\mathbf{Y} = i\mathbf{A}\mathbf{B}^{-1}$, is a Hermitian matrix, and for interfacial crack, we define

$$\mathbf{H} = \mathbf{Y}_{\mathrm{I}} + \bar{\mathbf{Y}}_{\mathrm{II}}$$

which is also Hermitian.

ε, κ and $\mathbf{\Lambda}$ are the eigenvalues and eigenvectors of

$$(\bar{\mathbf{H}} - \mathrm{e}^{2\pi\varepsilon}\mathbf{H})\Lambda = 0 \tag{A.11}$$

Let $\mathbf{H} = \mathbf{V} + \mathrm{i}\mathbf{F}$, where $\mathbf{V}$ is real and symmetric and $\mathbf{F}$ is real and antisymmetric, and $\mathbf{E} = \mathbf{F}\mathbf{V}^{-1}$, the results can therefore be expressed as

$$\begin{aligned} &\varepsilon = \frac{1}{\pi}\tanh^{-1}\omega_1; \quad \kappa = \frac{1}{\pi}\tan^{-1}\omega_2 \\ &\omega_1 = [(b^2 - c)^{1/2} - b]^{1/2}; \quad \omega_2 = [(b^2 - c)^{1/2} + b]^{1/2} \\ &b = \frac{1}{4}\mathrm{tr}[\mathbf{E}^2]; \quad c = \|\mathbf{E}\| \end{aligned} \tag{A.12}$$

ε, κ are the oscillatory indices. We also introduce the following expression (Nishioka and Shen, 2001)

$$\Lambda\,\mathrm{diag}[\mu_\alpha]\Lambda^{-1} = \mathbf{G}_1\mu_1 + \bar{\mathbf{G}}_1\mu_2 + \mathbf{G}_3\mu_3 + \mathbf{G}_4\mu_4 \tag{A.13}$$

where μ_α are arbitrary functions of z, and

$$\begin{aligned} \mathbf{G}_1 &= \frac{1}{2(\omega_1^2 + \omega_2^2)}\left\{[\omega_2^2\mathbf{I} - \mathbf{E}^2] + \mathrm{i}\omega_1^{-1}[\omega_2^2\mathbf{I} - \mathbf{E}^2]\mathbf{E}\right\} \\ \mathbf{G}_3 &= \frac{1}{2(\omega_1^2 + \omega_2^2)}\left\{[\omega_1^2\mathbf{I} + \mathbf{E}^2] - \omega_2^{-1}[\omega_1^2\mathbf{I} + \mathbf{E}^2]\mathbf{E}\right\} \\ \mathbf{G}_4 &= \frac{1}{2(\omega_1^2 + \omega_2^2)}\left\{[\omega_1^2\mathbf{I} + \mathbf{E}^2] + \omega_2^{-1}[\omega_1^2\mathbf{I} + \mathbf{E}^2]\mathbf{E}\right\} \end{aligned} \tag{A.14}$$

This expression is very useful in computation, because it avoids solving the eigen Eq. (A.11).

For interfacial crack,

$$\begin{aligned}\mathbf{f}_{\mathrm{I}}'(z) &= \frac{1}{\sqrt{2\pi z}}\mathbf{B}_{\mathrm{I}}^{-1}\Lambda\,\mathrm{diag}\left[z^{\mathrm{i}\varepsilon} \quad z^{-\mathrm{i}\varepsilon} \quad z^{k} \quad z^{-k}\right]\Lambda^{-1}\left[\mathbf{I}+\bar{\mathbf{H}}^{-1}\mathbf{H}\right]^{-1}\mathbf{K}\\ \bar{\mathbf{f}}_{\mathrm{II}}'(z) &= \frac{1}{\sqrt{2\pi z}}\mathbf{B}_{\mathrm{II}}^{-1}\Lambda\,\mathrm{diag}\left[z^{\mathrm{i}\varepsilon} \quad z^{-\mathrm{i}\varepsilon} \quad z^{k} \quad z^{-k}\right]\Lambda^{-1}\left[\mathbf{I}+\bar{\mathbf{H}}^{-1}\mathbf{H}\right]^{-1}\mathbf{K}\end{aligned} \tag{A.15}$$

in the upper half-space, and

$$\begin{aligned}\bar{\mathbf{f}}_{\mathrm{I}}'(z) &= \frac{1}{\sqrt{2\pi z}}\mathbf{B}_{\mathrm{I}}^{-1}\bar{\mathbf{H}}^{-1}\mathbf{H}\Lambda\,\mathrm{diag}\left[z^{\mathrm{i}\varepsilon} \quad z^{-\mathrm{i}\varepsilon} \quad z^{k} \quad z^{-k}\right]\Lambda^{-1}\left[\mathbf{I}+\bar{\mathbf{H}}^{-1}\mathbf{H}\right]^{-1}\mathbf{K}\\ \mathbf{f}_{\mathrm{II}}'(z) &= \frac{1}{\sqrt{2\pi z}}\mathbf{B}_{\mathrm{II}}^{-1}\bar{\mathbf{H}}^{-1}\mathbf{H}\Lambda\,\mathrm{diag}\left[z^{\mathrm{i}\varepsilon} \quad z^{-\mathrm{i}\varepsilon} \quad z^{k} \quad z^{-k}\right]\Lambda^{-1}\left[\mathbf{I}+\bar{\mathbf{H}}^{-1}\mathbf{H}\right]^{-1}\mathbf{K}\end{aligned} \tag{A.16}$$

in the lower half-space. Noting that the eigenvectors satisfy the orthogonality relation (Suo et al., 1992) and $(\mathbf{B}^{-1})^{\mathrm{T}}\mathbf{B}^{-1} = \mathrm{i}\mathbf{Y} - \mathrm{i}\bar{\mathbf{Y}}$

We can derive that

$$\mathbf{f}_{\mathrm{I}}'^{\mathrm{T}}(z)\mathbf{f}_{\mathrm{I}}'(z) - \bar{\mathbf{f}}_{\mathrm{II}}'^{\mathrm{T}}(z)\bar{\mathbf{f}}_{\mathrm{II}}'(z) = -\frac{\mathrm{i}}{4\pi z}\mathbf{K}^{\mathrm{T}}\mathbf{U}\mathbf{K} \tag{A.17}$$

Thus, Eq. (21) is obtained.

It is noted that all the formulas in this appendix suit for both static and dynamic interfacial cracks.

References

Beom, H.G., Atluri, S.N., 1996. Near-tip fields and intensity factors for interfacial cracks in dissimilar anisotropic piezoelectric media. Int. J. Fract. 75, 163–183.

Dascalu, C., Maugin, G.A., 1995. Dynamic fracture for piezoelectric material. Q. J. Mech. Appl. Math. 48, 237.

Eringen, A.C., Maugin, G.A., 1990. Electrodynamics of Continua I. Springer, New York, USA.

Gao, H., Zhang, T.Y., Tong, P., 1997. Local and global energy release rates for an electrically yielded crack in a piezoelectric ceramic. J. Mech. Phys. Solids 45, 491–510.

Hwu, C., 1993. Fracture parameters for the orthotropic bimaterial interface cracks. Eng. Fract. Mech. 45, 89–97.

Khutoryansky, N.M., Sosa, H., 1995. Dynamic representation formulas and fundamental solutions for piezoelectricity. Int. J. Solids Struct. 32, 3307–3325.

Kuo, C.M., Barnett, D.M., 1991. Modern Theory of Anisotropic Elasticity and Applications. In: Wu, J.J., Ting, T.C.T., Barnett, D.M. (Eds.). SIAM, p. 33.

Li, S., Mataga, P.A., 1996a. Dynamic crack propagation in piezoelectric materials-Part I. electrode solution. J. Mech. Phys. Solids 44, 1799–1830.

Li, S., Mataga, P.A., 1996b. Dynamic crack propagation in piezoelectric materials-Part II. vacuum solution. J. Mech. Phys. Solids 44, 1831–1866.

Lin, X., Ballmann, J., 1993. Re-consideration of Chen's problem by finite difference method. Eng. Fract. Mech. 44-5, t735–t739.

McMeeking, R.M., 1999. Crack tip energy release rate for a piezoelectric compact tension specimen. Eng. Fract. Mech. 64, 217–244.

Nishioka, T., Atluri, S.N., 1983. Path-independent integrals, energy release rates and general solutions of near-tip fields in mixed-mode dynamic fracture mechanics. Eng. Fract. Mech. 18, 1–22.

Nishioka, T., Shen, S., 2001. Higher order asymptotic solution for an interfacial crack in piezoelectric bimaterial under impact. Mater. Sci. Res. Int. 7, 157–165.

Nishioka, T., Shen, S., Yu, J.H., 2003. Dynamic J integral for dynamic interfacial cracks in piezoelectric bimaterials: formulation, material separation and component separation method. Int. J. Fract. 122 (3–4), 101–130.

Nishioka, T., Yasin, A., 1999. The dynamic J integral, separated dynamic J integrals and moving finite element simulations for subsonic, transonic and supersonic interfacial crack propagation. JSME Int. J. Ser. A 42, 25–39.

Park, S., Sun, C.T., 1995. Fracture criteria for piezoelectric ceramics. J. Am. Ceram. Soc. 78, 1475–1480.

Parton, V.Z., Kudriavtsev, B.A., 1988. Electromagnetoelasticity. Gordon and Breach, New York.

Shen, S., Kuang, Z.B., 1998. Interface crack in bi-piezothermoelastic media and the interaction with a point heat source. Int. J. Solids Struct. 35, 3899–3915.

Shen, S., Nishioka, T., 2000. Fracture of piezoelectric materials: energy density criterion. Theor. Appl. Fract. Mech. 33, 57–65.

Shen, S., Nishioka, T., 2003. Finite element simulation of impact interfacial crack problems in piezoelectric bimaterials. In: Yang, J., Maugin, G. (Eds.), Mechanics of Electromagnetic Solids. Kluwer Academic Publishers, pp. 211–227.

Shen, S., Nishioka, T., Kuang, Z.B., 1999. Impact interfacial fracture for piezoelectric ceramic. Mech. Res. Comm. 26, 347–352.

Shindo, Y., Ozawa, E., 1990. Mechanical Modeling of New Electromagnetic Materials. In: Hsieh, R.K.T. (Ed.). Elsevier Science Publishers B.V., p. 297.

Sun, K., Zhang, F.X., 1984. Piezoelectricity. Press of Denfense Industries, Beijing, China .

Suo, Z., Kuo, C.M., Barnett, D.M., Willis, J.R., 1992. Fracture mechanics for piezoelectric ceramics. J. Mech. Phys. Solids 40, 739–765.

Yau, J.F., Wang, S.S., 1984. An analysis of interface cracks between dissimilar isotropic materials using conservation integrals in elasticity. Eng. Fract. Mech. 20, 423–432.

Yeh, C.S., Shu, Y.C., Wu, K.C., 1993. Conservation laws in anisotropic elasticity I. Basic framework. Proc. R. Soc. Lond. A 443, 139–151.